Widespread immunogenic poly-epitope frameshift mutations in microsatellite unstable tumors

Vladimir Roudko[1,5 †], Cansu Cimen Bozkus[1 †], Theofano Orfanelli[3], Stephanie V. Blank[3], Benjamin Greenbaum[1,2,4,5 ‡], Nina Bhardwaj[1 ‡ *].

[1]*Department of Hematology and Medical Oncology, Icahn School of Medicine at Mount Sinai Hospital, New York, New York, USA;*

[2]*Department of Oncological Sciences, Icahn School of Medicine at Mount Sinai Hospital, New York, New York, USA;*

[3]*Department of Obstetrics, Gynecology and Reproductive Science, Icahn School of Medicine at Mount Sinai Hospital, New York, New York, USA;*

[4]*Department of Pathology, Icahn School of Medicine at Mount Sinai Hospital, New York, New York, USA;*

[5]*Center for Computational Immunology, Tisch Cancer Institute, Icahn School of Medicine at Mount Sinai Hospital, New York, New York, USA.*

[†]*These authors contributed equally to the work*

[‡]*These authors shared the last authorship*

[*]*Correspondence: nina.bhardwaj@mssm.edu (N.B.)*

Abstract

Microsatellite instability-high (MSI-H) tumors are an important model system for evaluating neoantigen-based immunotherapies given their high tumor mutation burden and response to checkpoint blockade. We identified tumor-specific, frameshift peptides, encoding multiple epitopes that originated from indel mutations shared among patients with MSI-H endometrial, colorectal and stomach cancers. Epitopes derived from these shared frameshifts have high population occurrence rates, wide presence in many tumor subclones and are predicted to bind to the most frequent HLA alleles in the TCGA MSI-H patient cohorts. Neoantigens arising from these mutations are more dissimilar to both self and viral antigens, indicating the creation of peptides, that, when translated, can present truly novel antigens to the immune system. Finally, we validated the immunogenicity of common frameshift peptides from MSI-H endometrial patients in an array of T cell stimulation experiments, using peripheral blood mononuclear cells isolated from healthy donors. Our study describes for the first time the widespread occurrence and strong immunogenicity of tumor-specific antigens, derived from shared frameshift mutations in MSI-H cancer and Lynch syndrome patients, suitable for the design of common preventive "off-the-shelf" cancer vaccines.

Introduction

Genetic alterations in tumor genomes that encode novel stretches of amino acids compared to normal cells are a potential source of immunogenic tumor-specific epitopes, commonly referred to neoantigens. Total neoantigen burden, (the sum of neoantigens predicted to be expressed by a tumor), has been demonstrated to be an independent proxy for response to anti-programmed cell death protein 1 (PD-1) immunotherapy[1–4]. However, determining neoepitopes in individual tumor sample remains fraught with uncertainties, such as the lack of congruence between selection of somatic variants and immunogenic neoantigens. Due to the presence of high loads of tumor-specific antigens, and strong effector T cell infiltration, microsatellite instability-high (MSI-H) tumors are an important model system for evaluating neoantigen-based immunotherapy in therapeutic and protective settings. The MSI-H tumor phenotype arises from defective DNA repair mechanisms due to a loss of the mismatch repair (MMR) activity. MSI-H is typically characterized by the variation of DNA length in microsatellite loci – units of one to ten mono-, di-, tri-, or tetra-nucleotides repeated multiple times[5]. In healthy cells these unpaired nucleotides are recognized and excised by MMR, but in MSI-H tumors they remain unrepaired. Some of these microsatellite regions are located in coding regions, where their destabilization may cause frameshift (fs-) mutations and thereby create a large somatic mutation burden, possessing a huge source of tumor-specific neoantigens.[4,5].

Inactivation of several MMR genes plays a key role in the acquisition of the MSI-H phenotype in hypermutated tumors[6–9]. This often happens at the later stages in tumorigenesis, and it originates by either deleterious somatic mutagenesis or epigenetic inactivation of MMR genes. This sporadic type of MSI-H tumors occurs in 10-40% of colorectal and endometrial cancers and is

mainly caused by biallelic hypermethylation of the MLH1 promoter[14,15]. Apart from somatic inactivation of MMR genes during tumorigenesis, germline mutations within the same genes are also found. Lynch syndrome, sometimes referred to hereditary nonpolyposis colorectal cancer (HNCC), is an inherited, autosomal-dominant disorder characterized by germline non-synonymous mutations in MRR genes, accounts for 3-5% of all colorectal and endometrial cancers. The majority of patients have germline mutations in the MSH2 (~30%) and PMS2 (~70%) genes[12]. Subjects with Lynch syndrome suffer from a high predisposition to develop cancer early life, with an 80% life time risk for colorectal or endometrial MSI-H cancers. Also estimates suggest as many as 1 in every 300 people may carry Lynch syndrome-associated germline alterations[13,14,15]. Epithelial tissues are primarily at risk of tumorigenesis, with colorectal cancers being the most common (80% of HNCC patients). The second most common cancer with a significant percentage of sporadic and hereditary-predisposed MSI-H type is endometrial carcinoma (60% of HNCC patients). The MSI-H group accounts for up to 28.6% of low-grade and 54.3% of high-grade endometrioid cancers. Other cancers such as bladder, gastric, ovarian, small bowel and renal are also somewhat predisposed[16].

Most neoantigens that are predicted from point mutations are derived from patient-specific passenger mutations, with most shared driver mutations creating rarely presented peptides[17]. Consequently, the former are preferentially applied in cancer vaccine platforms. However, the MSI-H phenotype has several features which can be leveraged for common “off the shelf” vaccine design: (1) a high-mutational burden in well-defined, limited sequence space – microsatellite regions; (2) a restricted pattern of the mutations due to nucleotide insertions or deletions; and (3) a high probability of shared indel mutations in protein coding genes, which

93 may induce formation of frameshift (fs-) peptide, which encodes multiple MHC-I restricted
94 epitopes (poly-epitope fs-peptide) that are shared among multiple patients[18,19]. Based on this
95 premise, we investigated fs-mutations in tumor genomes of MSI-H patients with colorectal,
96 stomach and endometrial carcinomas and identified a high frequency of broadly shared,
97 immunogenic, poly-epitope fs-peptides.
98

99 # Results

100 **MSI-H colorectal, stomach and endometrial patient cohorts have a high fs-load**
101 Though tumor evolution is primarily viewed as driven by a random mutational process, there is
102 accumulated evidence that some mutations are acquired non-randomly[40–43]. Considering the
103 existing skewness in mutational process and high load of indel mutations in microsatellite
104 regions within open reading frames of MSI-H tumors[23], we hypothesized MSI-H patients may
105 share mutational events. While missense somatic mutations share limited similarity across
106 multiple tumors[24,25], frameshift (fs-) mutations in microsatellite (MS) unstable regions are indeed
107 likely to generate common fs-peptides (**Supplement Figure 1A**). Though previous studies have
108 annotated somatic mutation load as well as the distribution and frequency of insertions/deletions
109 on a pan-cancer scale[17,18,26] (**Supplement Figure 1B**), little is known about the frequency of
110 shared mutational events. We examined mutational load in cancer cell lines from Cancer Cell
111 Line Encyclopedia[27,28] (CCLE) and found that fs-mutations are more frequenty shared among
112 multiple cancer cell lines, than missense mutations (**Supplement Figure 1C**).
113
114 The majority of TCGA tumors are microsatellite stable or their status is unknown. However,
115 ~20%-30% of endometrial, colorectal and stomach adenocarcinomas are diagnosed as

116 microsatellite unstable, MSI-H (UCEC, COAD, STAD respectively, **Figure 1A**). In total, the
117 MSI-H population in TCGA accounts for 338 patients (**Figure 1B**). The fs-load, as determined
118 by fs-mutation count per each patient, is particularly high in a subset of UCEC, COAD and
119 STAD patients (**Figure 1C**). Consistent with previous studies, the majority of frameshifts stems
120 from nucleotide deletions, as determined by correlating patient's fs-load with insertion-to-
121 deletion ratio (**Figure 1D**). Finally, the majority of fs-enriched patients are segregated according
122 to the clinical MSI-H biomarker, indicating nearly perfect specificity/selectivity of this
123 biomarker in detecting indel-enriched tumor types (**Figure 1E**).
124
125 **Colorectal, stomach and endometrial MSI-H adenocarcinomas are enriched in shared poly-**
126 **epitope fs-peptides**
127 We then hypothesized that de-novo translated peptide segments – fs-peptides – within a newly-
128 defined codon sequence frame (either +1 or +2) downstream of the indel mutation, may possess
129 a significant source of immunogenic class I neoepitopes. If such fs-derived neoepitopes exist,
130 they may also exhibit a high rate of turnover and processivity: mRNAs that encode frameshift
131 mutations may be rapidly degraded through the nonsense-mediated decay (NMD) pathway,
132 which is accompanied by nascent peptide decay on the 80S ribosome[29–33]. While the expression
133 of fs-genes may be downregulated, the translated product is destabilized, potentially producing
134 short, presentable peptides at a higher rate[34,35].
135
136 To identify potentially immunogenic epitopes derived from fs-mutations, we developed a fs-
137 neoantigen calling pipeline (see **Online Methods**). Using this pipeline, we analyzed the
138 distribution of fs-mutations, fs-peptides and corresponding fs-epitopes in MSI-H UCEC, COAD

and STAD cohorts of TCGA patients. As expected, we found that many genes were commonly mutated via indels in MS regions in all the three tumor types. Up to 80% of MSI-H COAD and STAD patients had several commonly mutated genes as a result of indels, e.g. ACVR2A, MIKI67, RPL22. More than 50% of MS-H UCEC patients shared a different set of genes affected by frameshifts e.g. CASP5, MUC6, KMT2C. Expectedly, the frequency of shared fs-peptides, derived from exactly the same fs-mutations, dropped, with only a few fs-peptides shared by 40% of MSI-H UCEC, or 50% of MSI-H COAD/STAD patients. Finally, the frequency of shared HLA epitopes in MSI-H UCEC patients approached 25% having 28 immunogenic fs-epitopes, and to 50% of COAD patients who had 29 shared epitopes (**Figure 2A, B**). Interestingly, colon and stomach MSI-H tumors had twice as many shared immunogenic fs-events than endometrial MSI-H tumors (**Figure 2B**), which likely stems from the different pathways of tumorigenesis, and from the profiles of mutated oncogene drivers.

To identify immunogenic fs-peptides with confidence, we developed a mutation ranking system based on maximization of four parameters (**Figure 2C**). Firstly, we introduced a quality metric for each called fs-mutation in which higher quality implies higher confidence that this mutation is truly somatic (**Supplement Figure 2A**). Also, we analyzed the distribution fs-peptide length: on average, the length of MSI-H frameshift peptides is 20-30 aminoacid (aa) residues, suggesting that these peptides may encode multiple immunogenic epitopes per fs-mutation (**Supplement Figure 2B**). Secondly, we maximized the number of putative neoepitopes per each fs-peptide: epitopes, predicted for each fs-peptide across all patients, were pooled and the total number of unique epitopes was determined. Thirdly, we grouped all HLA alleles predicted to bind those neoepitopes and considered this to be an HLA-ligandome of each fs-peptide. Maximization of

this parameter allowed us to pick poly-allelic fs-peptides, covering as diverse a set of HLA alleles in a population as possible. Finally, to include the population HLA allele frequency parameter, we quantified total amount of antigen-allele interactions per frameshift. Together, we ensured the prediction of fs-peptides that are most likely immunogenic, encode poly-epitopes, bind to a broad spectrum of HLA-alleles and widely shared. We identified 9, 37 and 23 fs-peptides derived from frequently shared indel mutations that encode poly-epitopes in endometrial, colorectal and stomach MSI-H patients, respectively (**Figure 2C**). Counting the number of epitopes derived from each fs-peptide in each patient showed a high level of presence of these epitopes in MSI-H cohort of patients. Alternatively, plotting the number of epitopes derived from frameshift sequence per each predicted HLA allele showed that many epitopes are predicted to bind to the most frequently expressed HLA alleles in the TCGA patient cohort (**Figure 2D**). Finally, among the detected fs-peptides, five were found in all MSI-H patients, pointing to the possibility to develop an off-the-shelf MSI-H vaccine for these three tumor types: SLC35F5, SEC31A, TTK, SETD1B and RNF43.

Nine poly-epitope fs-peptides shared in MSI-H endometrial carcinoma originate from clonal tumor-specific alleles and are correctly translated

We next focused our attention on frameshift-derived neoantigens from MSI-H endometrial carcinoma, as these have not been characterized to date. At least two neoepitopes from nine selected fs-peptides are detected in >95% of the MSI-H UCEC TCGA patient cohort. Moreover, binding profiles of the predicted epitopes cover almost all HLA-alleles of the same patient population as well as targeting the majority of frequent HLA types (**Figure 2D**). Importantly, only the “mixture” of MHC-I epitopes derived from all 9 peptides has the potential to reach a

significantly high representation of all HLA allele-epitope diversity, than each fs-peptide separately (**Figure 3A**).

Additionally, we analyzed the tumor allele frequencies from the MSI-H UCEC patient cohort to estimate the abundance of the selected nine shared frameshifts in tumor genomes. To do that, we compared corresponding fs-allele frequencies in normal and tumor samples. As expected, fs-alleles are barely detectable in normal tissues, but in tumor biopsies their frequencies rise up to 40% on average in tumor biopsies, indicating these mutations are often clonal (**Figure 3B**). This suggests the 9-peptide mix has a potential to prime T cell responses against almost all malignant cells. However, the high mutation rates of MSI-H tumors might decrease the probability of the shared fs-peptides being translated (**Supplementary Figure 2C**). Taking this into consideration, we assessed the conditional probability of shared fs-peptide being correctly translated given this shared mutation has happened. For this purpose, we estimated all disruptive upstream and downstream mutation frequencies using the MSI-H TCGA patients and calculated posterior probabilities (**Supplementary Figure 2D**). Though the majority of MSI-H UCEC shared fs-peptides has a high probability of being correct (>0.9), TTK and RNF43 frameshifts have an increased chance of being inactivated, with a ~0.8 probability of being correct.

The predicted nine shared poly-epitope fs-peptides are expressed in MSI-H UCEC patients

To estimate the expression level of genes encoding shared fs-peptides, we analyzed RNA expression derived from TCGA RNAseq samples of matched MSI-H patients (**Figure 3C-F**). We performed unsupervised clustering of MSI-H patients by genes with predicted shared fs-events, obtaining the patient and gene rankings according to the shared fs-load (**Figure 3C**). We

208 then plotted FPKM expression values of genes encoding shared fs-peptides, and ranked them
209 according to the previously obtained patient and gene rankings (**Figure 3C**). We observed no
210 correlation between RNA expression and shared fs-load, suggesting that frameshifted genes are
211 not selectively epigenetically silenced in tumors (**Figure 3D**). We next analyzed the expression
212 of nine shared fs-mutations in MSI-H UCEC patients. As two of the shared fs-mutations are
213 present in one gene, formally we detected 8 uniquely mutated genes, and six of these were
214 expressed at the RNA level from matching tumor samples (**Figure 3E**). To assess the expression
215 level of fs-alleles, we compared the normalized read count containing the indel with total amount
216 of reads covering the targeted genomic loci from MSI-H RNAseq samples and MSS samples as a
217 control (**Figure 3E)**. We detected statistically significant and robust expression of fs-alleles in
218 MSI-H patients (**Figure 3E**). Also, we showed representative RNAseq expression histograms,
219 covering the predicted shared frameshift in RNF43 gene, and derived indel RNAseq read
220 frequencies in MSI-H and MSS patients (**Figure 3F**). Thus, we confirmed that fs-alleles are
221 indeed expressed and detected in bulk RNAseq.
222
223 We then tested if high load of shared poly-epitope fs-mutations had a survival benefit within the
224 MSI-H patient cohort and/or may be skewed towards later tumor stage. This questions is
225 important for ongoing immunotherapy trials, where MSI-H becomes widely accepted as a
226 predictive biomarker to anti-PD-1 therapy[36,37], although deeper genetic differences between
227 patients may underlie the incomplete responsiveness. For this purpose, we performed Cox
228 regression and survival analyses of TCGA MSI-H UCEC patients stratified by shared fs-load, as
229 high and low, and analyzed tumor stage and patient age in the same strata. Patient age and tumor
230 stage were evenly represented in both, fs-high and fs-low MSI-H cohorts (**Supplemental Figure**

3). Finally, we did not detect any significant benefit in patients' survival based on shared fs-load in any of the MSI-H tumor types (**Supplementary Figure 4**).

Tumor fs-epitopes are more likely to be presented and are less similar to viral antigens than missense derived epitopes

We next examined the intrinsic properties of fs-derived epitopes when compared to missense-derived epitopes and viral antigens. In previously published studies, similarity of tumor-derived neoantigens to pathogen derived (viral) antigens has been shown to be predictive in the checkpoint blockade immunotherapy setting[1,2]. First, we calculated the total amount of neoantigens derived from missense mutations of MSI-H patients and compared it to fs-epitope load. Despite the fact that the total frameshift and the missense mutation loads were similar, the number of MHC-I epitopes per mutation were different: 4 epitopes per one frameshift and 2 per one missense mutation on average (**Supplement Figure 5A**). This observation suggests, that fs-mutations may be more immunogenic then missense due to an increased probability of presentation. While most of missense-derived epitopes are, by definition, one aa different from a self-peptide, the majority of fs-derived epitopes are unique, "non-host" peptide sequences and hence exhibit minimal similarity to the human proteome (**Supplement Figure 3B**). This implies, that fs-derived epitopes might have never been tolerized by the host immune system, and that the frameshift-specific T-cells may have little or minimal autoreactivity.

We also compared these two epitope datasets with virus-derived antigens. At multiple search parameters, the overall number of missense epitopes, when matched with viral ones, was higher, than matched fs-epitopes (**Supplement Figure 3C**). We speculate this observation is due to the

overall viral adaptation to the human proteome and host T-cell epitopes, as viruses need to hijack particular host functionalities in order to interact with the host cellular machinery as well as escape host immune recognition. As a consequence of this finding, we conclude fs-epitopes appear "less self' than either missense or virus derived epitopes.

Predicted shared poly-epitope fs-peptides are detected and expressed in diverse set of cancer cell lines from CCLE

To validate the predicted shared fs-mutations in an external dataset, we verified the presence of these mutations in the Cancer Cell Line Encyclopedia (CCLE) (**Figure 4**). 34 from 45 of predicted shared poly-epitope fs-peptides were detected in multiple cancer cell lines, derived from different tumor types. Diverse cancer cell lines had different numbers of shared fs-peptides, e.g. intestine, endometrium, stomach and prostate cancer cell lines having 5-10 shared fs-mutations per cell line, while hematopoietic, ovarian and lung cancer cell lines had 1-5 shared fs-mutations per cell line (**Figure 4A**). The presence of predicted shared fs-mutations in the last three tumor types suggests a broader occurrence of shared poly-epitope fs-peptides across tumors, than initially suggested. The frequency of shared fs-positive cell lines per tissue type was around 20, 40 and 60% of intestine, stomach and endometrial cell lines (Figure 4B). Interestingly, the majority of fs-mutations differentially shared by MSI-H UCEC, COAD and STAD TCGA tumors were evenly detected in endometrial, intestine and stomach cancer cell lines (**Figure 4C**), suggesting epigenetic remodeling of certain chromatin areas making them accessible for genome destabilization. Initially predicted in TCGA, shared fs-peptides were the only fs-mutations statistically significantly shared in cancer cell lines than any other fs-mutation derived from the same genes (**Figure 4D**). Fs-allele coverage analysis suggested that predicted

shared fs-mutations are clonal and present in shared fs-positive cancer cell lines at 30-50% allele frequency on average (**Figure 4E**). Also, RNAseq data indicates the gene expression patterns are unchanged upon acquiring shared frameshift (**Supplement Figure 6**). Overall, the CCLE dataset analysis confirms the widespread occurrence of predicted shared fs-peptides in cancer.

Nine poly-epitope fs-peptides shared in MSI-H UCEC patients are highly immunogenic

To assess the immunogenicity of the nine predicted fs-peptides from MSI-H UCEC patient cohort, we evaluated the T cell responses against each neopeptide using a T cell immunogenicity assay developed in our laboratory that is designed to rapidly prime naïve T cells (see **Online Methods**). In brief, long overlapping peptide (OLP) libraries spanning each fs-peptide were designed (**Supplementary Figure 7**). Using these OLP pools, T cells from 15 randomly picked healthy donors (HD) were primed and expanded. After expansion, the cells were stimulated with the OLP pools and fs-peptide-specific T cell responses were evaluated by measuring IFN-γ production using ELISPOT (**Figure 5A**). Results showed that each fs-peptide could elicit T cells responses in a subset of subjects tested. Furthermore, some subjects had reactive T cells against multiple fs-peptides (**Figure 5B-D**). Importantly, when combined, the fs-peptide-specific T cells were significantly enriched in the subject cohort in accordance with the predictions detailed in Figure 2D. We also characterized the fs-peptide-specific T cell responses in the same HD cohort by intracellular staining (ICS). Results from both assays showed similar stimulation profiles. Moreover, responses to fs-peptides were observed primarily in CD8+ T cells, reaching up to 10% of T cells indicating strong priming to these neoantigens. (**Figure 5E-G**). In total, a majority of HD (13 out of 15) responded to at least one fs-peptide. Importantly, the reactive T cells produced TNF-α, in addition to IFN-γ, suggesting that fs-peptide-specific T cells are polyfunctional

(**Supplementary Figure 8**). Additionally, we synthesized control peptides (15-aa) for each fs-peptide using their wild type sequence surrounding the fs-mutation site. Responses by HD T cells to stimulation with WT OLP pool were not higher than the background (**Figure 5H**), suggesting that the observed T cell responses were specific to fs-peptides. Next, we investigated whether the fs-peptide-specific T cells responses that were observed in the HD cohort correlated with the predicted high affinity epitope load. To determine the predicted epitope load, we identified the HLA-I alleles of each subject by sequence-based HLA-I genotyping and investigated the predicted binding affinity of epitopes from fs-peptides to each subject's unique HLA. We found no significant correlation between the total epitope load per patient and experimentally observed response rate (**Figure 5I-K**). This observation is expected since many studies have reported that the majority of predicted epitopes fail to elicit T cell responses[38] and that high HLA-peptide binding affinity does not equate to immunogenicity. Altogether, our data show that MSI high patients have an increased frequency of high-quality T cell epitopes derived from shared fs-peptides, binding to a broad spectrum of HLA alleles, capable of inducing immunogenicity for CD8+ T cell in particular.

Discussion

In this study we evaluated the MSI-H patients from the TCGA database for the presence of shared, immunogenic tumor-associated neoantigens, providing a basis for the design of a common "off-the-shelf" cancer vaccine. We proposed fs-events to have a high probability of being shared across multiple MSI-H patients. To this end, we characterized the MSI-H population and the tumor genomic frequencies of corresponding indel mutations, as well as their tumor expression profiles. Our approach to detect immunogenic, shared neoantigens relies on

two assumptions: (i) indel mutations occurring in frequently mutated MS regions will lead to identical fs-peptide extensions, (ii) these frequent, identical fs-peptide extensions encode poly-epitopes with broad HLA allele specificity. We confirmed the validity of our neoantigen selection approach by testing the immunogenicity of the selected fs-peptides. We found that the selected peptides were highly immunogenic and generated strong CD3+CD8+ T cell responses in a broad range of subjects.

One important finding is the existence of shared mutations that generate immunogenic neoantigens. Indeed, the majority of tumors develop a restricted profile of mutations, either disrupting activity of oncosuppressors, like p53 and KREB, or promoting gain-of-function activity of oncogenes, like BRAF V600E. However, these shared mutations often escape immune recognition and are less likely to encode tumor-associated neoantigens[17]. By contrast, in MSI-H tumors indel mutagenesis is generally restricted to MS regions, thus increasing the probability of being shared among patients (**Supplement Figure 1A, B**). Another key observation is that indel mutations in MS within protein coding regions are more likely to produce common fs-peptide, which may encode immunogenic neoantigens. With an average length of 15 – 50 aa residues, frameshift extensions can easily accommodate multiple 9-mer T cell epitopes. By running conventional antigen-prediction pipelines, we annotated several shared fs-peptides as immunogenic.

From the tumor's evolutionary perspective, there is no need to keep those immunogenic mutations, so multiple tumor-intrinsic escape mechanisms might exist as a consequence. As described elsewhere, MSI-H tumors upregulate checkpoint molecules to evade the development

of antitumor T cell responses[12,26,37,39]. Blockade of this mechanism has been proven to be effective in clearing a range of MSI-H tumors in multiple clinical trials[37,40]. However, several other immune resistance mechanisms might exist: downregulation of HLA-allele and/or β-microglobulin expression; inactivation/loss of antigen processing genes; inactivation/loss of interferon-γ-response pathway genes; disruption of immunogenic neoantigens by additional, acquired mutations[41–43]. The latter have been examined by us with respect to mutational escape of shared poly-epitope fs-peptides. Indeed, in certain cases we observed mutations that were potentially disruptive to the predicted neoantigens (**Supplementary Figure 2**). Another important finding is the high-occurrence of predicted shared fs-peptides in commonly utilized cancer cell lines (CCLE, **Figure 4**). We therefore suggest the potential utility of these shared fs-positive cell lines in immunological studies of predicted fs-epitopes, such as understanding the efficacy of antigen-dependent tumor cell killing as well as studying prospective tumor-escape mechanisms.

Finally, we investigated the sequence space produced by fs-mutations. Previous reports provided evidence that high quality immunogenic neoantigens are related to viral epitope sequences and are predictive for outcome of checkpoint blockade immunotherapy[1,2]. To determine whether the same rules applied to fs-derived neoantigens, we investigated similarities between viral epitopes and immunogenic neoantigens. We found missense-derived neoantigens to be 3 times more similar to viral epitopes than fs-neoantigens. We attributed this to viruses evolving within the cellular environment of their host, trying to mimic the host's functionalities and potentially avoid immune responses through extensive similarity to the host proteome. The fs-mutations are therefore even "further from self" than viral antigens (**Supplemental Figure 3**). Taken together,

we conclude that frameshifts represent unique, intrinsically different epitope space, with a great potential for discovering immunogenic epitopes which can be targeted by immune therapies. In a recently published study authors investigated the presence of fs-derived neoepitopes in TCGA and arrived at similar conclusions[44]. Also, a few previous reports investigated the immunogenicity of unique fs-mutations on a small scale[45–49]. In addition to this shared research goal, our group performed in depth computational characterization and experimental validation of shared fs-epitopes in MSI-H tumors specifically.

Preselected fs-mutations might also be used for developing targeted sequencing panels for diagnostic purposes. Precise detection and mapping of predicted mutations in each tumor patient may enhance the chances of achieving a positive response with an applied vaccine. The usage of targeted sequencing panels for diagnostics have already proven essential for developing actionable treatments, particularly in the selection of targeted regimens. We believe the same paradigm will become useful for precise immunotherapies, with physicians being able to select the ideal cancer vaccine formulation based on the results of targeted sequencing panels.

Our work revealed the possibility of designing common cancer vaccines in specific tumor subtypes with broad HLA-allele specificity. By applying tailored vaccines for MSI-H endometrial, colorectal and stomach carcinomas, one can potentially achieve immunological responses against existing neoplasms or develop preventive memory T cell responses in high-risk patient populations, like those with Lynch syndrome.

Online Methods

392 **Computational analysis of mutational data from TCGA**

393 Tumor-associated antigens were predicted using somatic mutation datasets, called by internal
394 mutation pipelines of The Cancer Genome Atlas (TCGA, or Genomics Data Commons,
395 https://gdc.cancer.gov). Briefly, annotated somatic missense and frameshift mutations by Mutect,
396 Somatic Sniper, Varscan and Muse were combined together per each patient. In case of somatic
397 missense mutations, corresponding 17-aminoacid residue-length normal peptides, surrounding
398 mutation site, were converted to tumor-specific peptides and used for MHC-I epitope prediction.
399 In case of frameshift mutations, the tumor specific peptide was called as following: major
400 mRNA isoform was mutated according to the frameshift mutation, translated starting from "-8"
401 aminoacid residue position from the mutation site till the stop codon within the new open reading
402 frame, defined by the frameshift. Resulting frameshift peptides were used for MHC-I epitope
403 prediction. NetMHC v4.0 and NetMHCpan v3.0[50,51] were used to predict missense and
404 frameshift epitopes. HLA allele types for >5000 patients from TCGA were taken from
405 previously published paper[3]. Collected epitope data was analyzed using statistical packages,
406 available in Prism and R, using custom written scripts.
407
408 **Expression analysis of TCGA**
409 Hg19-aligned RNAseq bam files were downloaded from GDC (https://gdc.cancer.gov). Obtained
410 .bam files were processed with samtools to extract RNAseq reads, covering 250 nt genomic loci
411 around shared fs-mutation (samtools view -b -L chr19.region.bed $i/*.bam >
412 $filename.chr19.bam). To count indel events in extracted RNAseq bam fiels, we applied
413 samtools mpileup tool: samtools mpileup -uf /work/scratch/index/TCGA/GRCh38.d1.vd1.fa $i |

bcftools view -l region.bed - | grep "INDEL" >> $filename.vcf. Finally, obtained data was processed with custom scripts and analysed in PRISM 8.

Peptide comparison with virus epitope databases

The collection of viral MHC-I epitopes was downloaded from IEDB database and preformatted for BLAST usage (makeblastdb -in iedb.fasta -parse_seqids -dbtype prot). Predicted frameshift and missense originated T-cell epitopes form MSI-H patients were BLASTed against IEDB. For comparison with viral we used following command: blastp -db iedb.fasta -query frameshift.neoantigen.netMHC.score.fasta -outfmt "6 qseqid sseqid pident ppos positive mismatch gapopen length qlen slen qstart qend sstart send qseq sseq evalue bitscore" -word_size 3 -gapopen 32767 -gapextend 32767 -evalue 1 -max_hsps_per_subject 1 -matrix BLOSUM62 -max_target_seqs 10000000 -out frameshift.neoantigen.iedb.blast.out. To compare predicted epitopes with human proteome, we used last command. First, we preformatted human proteome (ensemble archive from December 2016): lastdb -p human.proteome human.proteome.fasta. Then we used following command to compare epitopes to this database: lastal -f MAF -r 2 -q 1 -m 100000000 -a 100000 -d 15 -l 4 -k 1 -j1 -P 10 human.proteome frameshift.neoantigen.netMHC.score.fasta > frameshift.neoantigen.human.last.out. Finally, obtained results were processed with custom scripts (bash, python) and analyzed in PRISM 8.

Computational analysis of CCLE database

Somatic mutation data and normalized RNAseq expression values for genes with shared fs-mutations were obtained from https://portals.broadinstitute.org/ccle. Total mutation counts per

all cell lines were taken from CCLE_DepMap_18q3_maf_20180718.txt. Obtained data was processed with custom scripts and analyzed in PRISM 8.

Code availability

The scripts and code are freely available on git account: https://github.com/VladimirRoudko

Peptide synthesis

Custom peptide libraries for WT and mutated peptides were chemically synthesized by GenScript (USA/China). Each peptide had >80% purity as determined by high performance liquid chromatography. MOG and CEFT peptide pools were commercially available at JPT Peptide Technologies (Germany). Each peptide was resuspended in DMSO and used at a final concentration of 1 µg/mL. Sequences of mutated peptides are displayed in supplemental figure 7 and the WT sequences are as follows: for SLC35F5 GKLTATQVAKISFFF, for SEC31A QAVQSQGFINYCQKK, for SLC22A9 LEILKSTMKKELEAA, for TTK ESHNSSSSKTFEKKR and YSGGESHNSSSSKTF, for SETD1B MENSHPPHHHHQQPP, for OR7E24 MSYFPILFFFFLKRC, for RNF43 KSSLSARHPQRKRRG and for ASTE1 AEIFLPKGRSNSKKK.

Rapid T-cell activation protocol

Healthy donor PBMCs were cultured in X-VIVO15 media (LONZA) with cytokines promoting dendritic cell (DC) differentiation overnight and then stimulated with peptide pool as displayed in supplemental figure 7 (each peptide at 1 µg/mL) in the presence of adjuvant promoting DC maturation in X-VIVO15. Stimulation with DMSO (vehicle) and MOG pool (JPT, 1 µg/mL)

were used as negative controls and CEFT pool (JPT, 1 μg/mL) were used as positive controls. Next day, cells were fed with IL-2 (R&D Systems, 10 IU/mL) and IL-7 (R&D Systems, 10 ng/mL) in RPMI media (Gibco) containing 10% human serum. Cells were fed every 2-3 days. IL-2 and IL-7 were not added at the last feeding. After 10 days of culture, cells were harvested and re-stimulated with peptides (1 μg/mL) in the presence of anti-CD28 (0.5 mg/mL) and anti-CD49d (0.5 mg/mL) antibodies. Where indicated, cells were stimulated with PMA (Sigma-Aldrich, 50 ng/mL) and ionomycin (Sigma-Aldrich, 1 μg/mL), as positive control. IFN-γ formation was measured by flow cytometry or ELISPOT. For flow cytometry, 1 hour after re-stimulation with peptides, cells were added BD GolgiStop™, containing monensin and BD GolgiPlug™, containing brefeldin A according to manufacturer's suggestion. IFN-γ production was measured 12-hours after the addition of protein transport inhibitors by intracellular staining usingBD Cytofix/Cytoperm™ reagents according to manufacturer's protocol. For ELISPOT analysis, cells were re-stimulated in plates with mixed cellular ester membrane that were coated with anti-IFN-γ antibody (Mabtech, 4 μg/mL). Plates were processed for IFN-γ detection after 48-hours of culture.

Author Contributions

N.B. and S.B. initiated the project; N.B, V.R., C.C.B and T.O. designed the study; C.C.B. collected the samples; V.R and C.C.B. acquired and analyzed data. N.B, B.G., V.R., C.C.B and T.O interpreted the data; V.R. and C.C.B. wrote the manuscript; V.R., C.C.B., S.B., B.G. and N.B. revised the manuscript.

Competing Interests

N.B. receives research funds from Novocure, Celldex, Ludwig institute, Genentech, Oncovir, Melanoma Research Alliance, Cancer Research Institute, Leukemia & Lymphoma Society, NYSTEM, Regeneron, and is on the advisory boards of Neon, Tempest, Checkpoint Sciences, Curevac, Primevax, Novartis, Array BioPharma, Roche, Avidea; N.B. receives grant support and serves on advisory board at Parker Institute for Cancer Immunotherapy; N.B. has National Institutes of Health grants R01CA201189, R01CA180913 and R01AI081848

B.G. has National Institutes of Health grants 7R01AI081848-04 and 1P30CA196521-01; B.G. has Stand Up To Cancer–National Science Foundation–Lustgarten Foundation Convergence Dream Team Grant sponsored by Stand Up to Cancer, the Lustgarten Foundation, the V Foundation and the National Science Foundation grant NSF 1545935; B.G. is The Pershing Square Sohn Prize—Mark Foundation Fellow supported by funding from The Mark Foundation for Cancer Research.

References

1. Luksza, M. *et al.* A neoantigen fitness model predicts tumour response to checkpoint blockade immunotherapy. *Nature* **551**, 517–520 (2017).
2. Balachandran, V. P. *et al.* Identification of unique neoantigen qualities in long-term survivors of pancreatic cancer. *Nature* **551**, S12–S16 (2017).
3. Charoentong, P. *et al.* Pan-cancer Immunogenomic Analyses Reveal Genotype-Immunophenotype Relationships and Predictors of Response to Checkpoint Blockade: Cell Reports. *Cell Rep.* **18**, 248–262 (2017).
4. Hugo, W. *et al.* Genomic and Transcriptomic Features of Response to Anti-PD-1 Therapy in Metastatic Melanoma. *Cell* **165**, 35–44 (2016).

505 5. Kim, T. M., Laird, P. W. & Park, P. J. The landscape of microsatellite instability in
506 colorectal and endometrial cancer genomes. *Cell* **155**, 858–868 (2013).
507 6. Walther, A. *et al.* Genetic prognostic and predictive markers in colorectal cancer. *Nat.*
508 *Rev. Cancer* **9**, 489–499 (2009).
509 7. Ahmed, D. *et al.* Epigenetic and genetic features of 24 colon cancer cell lines.
510 *Oncogenesis* **2**, 1–9 (2013).
511 8. Diaz-Padilla, I. *et al.* Mismatch repair status and clinical outcome in endometrial cancer:
512 A systematic review and meta-analysis. *Crit. Rev. Oncol. Hematol.* **88**, 154–167 (2013).
513 9. Zighelboim, I. *et al.* Microsatellite instability and epigenetic inactivation of MLH1 and
514 outcome of patients with endometrial carcinomas of the endometrioid type. *J. Clin. Oncol.*
515 **25**, 2042–2048 (2007).
516 10. Veigl, M., Kastury, L., Olechnowicz, J., Ma, A. & Markowitz, S. Biallelic inactivation of
517 hMLH 1 by epigenetic gene silencing , a novel mechanism causing human MSI cancers.
518 *PNAS* **95**, 8698–8702 (1998).
519 11. Cunningham, J. M. *et al.* Hypermethylation of the hMLHl Promoter in Colon Cancer with
520 Microsatellite Instability. (1998).
521 12. Gatalica, Z., Vranic, S., Xiu, J. & Swensen, J. High microsatellite instability (MSI-H)
522 colorectal carcinoma : a brief review of predictive biomarkers in the era of personalized
523 medicine. *Fam. Cancer* **15**, 405–412 (2016).
524 13. Chung, D. C. & Rustgi, A. K. The Hereditary Nonpolyposis Colorectal Cancer Syndrome:
525 Genetics and Clinical Implications. *Ann. Intern. Med.* **138**, (2019).
526 14. Carethers, J. M. *et al.* Advances in Colorectal Cancer Lynch syndrome and Lynch
527 syndrome mimics : The growing complex landscape of hereditary colon cancer. *World J.*

Gastroenterol. **21**, 9253–9261 (2015).

15. Cohen, S. A., Pritchard, C. C. & Jarvik, G. P. Lynch Syndrome : From Screening to Diagnosis to Treatment in the Era of Modern Molecular Oncology. *Annu. Revew Genomics Hum. Genet.* **20**, 1–15 (2019).

16. Vasen, H. F. A. *et al.* Cancer Risk in Families With Hereditary Nonpolyposis Colorectal Cancer Diagnosed by Mutation Analysis. *Gastroenterology* **110**, 1020–1027 (1996).

17. Marty, R. *et al.* MHC-I Genotype Restricts the Oncogenic Mutational Landscape. *Cell* **0**, 1–12 (2017).

18. Turajlic, S. *et al.* Insertion-and-deletion-derived tumour-specific neoantigens and the immunogenic phenotype: a pan-cancer analysis. *Lancet Oncol.* **18**, 1009–1021 (2017).

19. Nangalia, J. *et al.* Somatic CALR mutations in myeloproliferative neoplasms with nonmutated JAK2. *N. Engl. J. Med.* **369**, 2391–2405 (2013).

20. Iranzo, J., Martincorena, I. & Koonin, E. V. Cancer-mutation network and the number and specificity of driver mutations. *PNAS* **115**, 6010–6019 (2018).

21. Buljan, M., Blattmann, P. & Aebersold, R. Systematic characterization of pan-cancer mutation clusters. *Mol. Syst. Biol.* **14**, 1–19 (2018).

22. Gerstung, M. *et al.* Universal Patterns of Selection in Cancer and Somatic Tissues. *Cell* **171**, 1029–1041 (2017).

23. Cortes-Ciriano, I., Lee, S., Park, W. Y., Kim, T. M. & Park, P. J. A molecular portrait of microsatellite instability across multiple cancers. *Nat. Commun.* **8**, 1–12 (2017).

24. Schumacher, T. N. & Schreiber, R. D. Neoantigens in cancer immunotherapy. *Science (80-.).* **348**, 69–74 (2015).

25. Mcgranahan, N. *et al.* Clonal neoantigens elicit T cell immunoreactivity and sensitivity to

immune checkpoint blockade. *Science (80-.).* **351**, 1463–1469 (2016).

26. Mlecnik, B. *et al.* Integrative Analyses of Colorectal Cancer Show Immunoscore Is a Stronger Predictor of Patient Survival Than Microsatellite Instability. *Immunity* **44**, 698–711 (2016).

27. Ghandi, M., Huang, F., Garraway, L. A. & Sellers, W. R. Next-generation characterization of the Cancer Cell Line Encyclopedia. *Nature* (2019). doi:10.1038/s41586-019-1186-3

28. Barretina, J. *et al.* The Cancer Cell Line Encyclopedia enables predictive modelling of anticancer drug sensitivity. *Nature* **483**, 4–11 (2012).

29. Frischmeyer, P. A. *et al.* An mRNA surveillance mechanism that eliminates transcripts lacking termination codons. *Science* **295**, 2258–61 (2002).

30. Schweingruber, C., Rufener, S. C., Zünd, D., Yamashita, A. & Mühlemann, O. Nonsense-mediated mRNA decay - mechanisms of substrate mRNA recognition and degradation in mammalian cells. *Biochim. Biophys. Acta* **1829**, 612–23 (2013).

31. Isken, O. & Maquat, L. E. The multiple lives of NMD factors: balancing roles in gene and genome regulation. *Nat. Rev. Genet.* **9**, 699–712 (2008).

32. Conti, E. & Izaurralde, E. Nonsense-mediated mRNA decay: Molecular insights and mechanistic variations across species. *Curr. Opin. Cell Biol.* **17**, 316–325 (2005).

33. Kurosaki, T., Popp, M. W. & Maquat, L. E. Quality and quantity control of gene expression by nonsense-mediated mRNA decay. *Nat. Rev. Mol. Cell Biol.* (2019). doi:10.1038/s41580-019-0126-2

34. Apcher, S. *et al.* Major source of antigenic peptides for the MHC class I pathway is produced during the pioneer round of mRNA translation. *Proc. Natl. Acad. Sci. U. S. A.* **108**, 11572–7 (2011).

574 35. Buchwald, G. *et al.* Insights into the recruitment of the NMD machinery from the crystal
575 structure of a core EJC-UPF3b complex. *Proc. Natl. Acad. Sci. U. S. A.* **107**, 10050–10055
576 (2010).
577 36. Dudley, J. C., Lin, M. T., Le, D. T. & Eshleman, J. R. Microsatellite instability as a
578 biomarker for PD-1 blockade. *Clin. Cancer Res.* **22**, 813–820 (2016).
579 37. Le, D. T. *et al.* PD-1 Blockade in Tumors with Mismatch-Repair Deficiency. *N. Engl. J.*
580 *Med.* **372**, 2509–2520 (2015).
581 38. Editorial. The problem with neoantigen prediction. *Nat. Biotechnol.* **35**, 97–97 (2017).
582 39. Mittica, G., Ghisoni, E., Giannone, G., Aglietta, M. & Valabrega, G. Checkpoint
583 inhibitors in endometrial cancer : preclinical rationale and clinical activity. *Oncotarget* **8**,
584 90532–90544 (2017).
585 40. Le, D. T. *et al.* Mismatch repair deficiency predicts response of solid tumors to PD-1
586 blockade. *Science (80-.).* **413**, 409–413 (2017).
587 41. Gao, J. *et al.* Loss of IFN-γ Pathway Genes in Tumor Cells as a Mechanism of Resistance
588 to Anti-CTLA-4 Therapy. *Cell* **167**, 397-404.e9 (2016).
589 42. Sharma, P., Hu-Lieskovan, S., Wargo, J. A. & Ribas, A. Primary, Adaptive, and Acquired
590 Resistance to Cancer Immunotherapy. *Cell* **168**, 707–723 (2017).
591 43. Roh, W. *et al.* Integrated molecular analysis of tumor biopsies on sequential CTLA-4 and
592 PD-1 blockade reveals markers of response and resistance. *Sci. Transl. Med.* **9**, (2017).
593 44. Koster, J. & Plasterk, R. H. A. A library of Neo Open Reading Frame peptides (NOPs) as
594 a sustainable resource of common neoantigens in up to 50 % of cancer patients. *Sci. Rep.*
595 1–8 (2019). doi:10.1038/s41598-019-42729-2
596 45. Garbe, Y., Maletzki, C. & Linnebacher, M. An MSI Tumor Specific Frameshift Mutation

in a Coding Microsatellite of MSH3 Encodes for HLA-A0201-Restricted CD8+ Cytotoxic T Cell Epitopes. *PLoS One* **6**, 2–9 (2011).

46. Maletzki, C., Schmidt, F., Dirks, W. G., Schmitt, M. & Linnebacher, M. Frameshift-derived neoantigens constitute immunotherapeutic targets for patients with microsatellite-instable haematological malignancies: Frameshift peptides for treating MSI+ blood cancers. *Eur. J. Cancer* **49**, 2587–2595 (2013).

47. Wagner, S., Mullins S, C. & Linnebacher, M. Colorectal cancer vaccines: Tumor-associated antigens vs neoantigens. *World J. Gastroenterol.* **24**, 5418–5432 (2018).

48. Schwitalle, Y. *et al.* Immune Response Against Frameshift-Induced Neopeptides in HNPCC Patients and Healthy HNPCC Mutation Carriers. *Gastroenterology* **134**, 988–997 (2008).

49. Woerner, S. M. *et al.* Pathogenesis of DNA repair-deficient cancers: A statistical meta-analysis of putative Real Common Target genes. *Oncogene* **22**, 2226–2235 (2003).

50. Andreatta, M. & Nielsen, M. Gapped sequence alignment using artificial neural networks: application to the MHC class I system. *Bioinformatics* **32**, 511–517 (2016).

51. Nielsen, M. & Andreatta, M. NetMHCpan-3.0; improved prediction of binding to MHC class I molecules integrating information from multiple receptor and peptide length datasets. *Genome Med.* **8**, 1–9 (2016).

Figures and Tables

A.

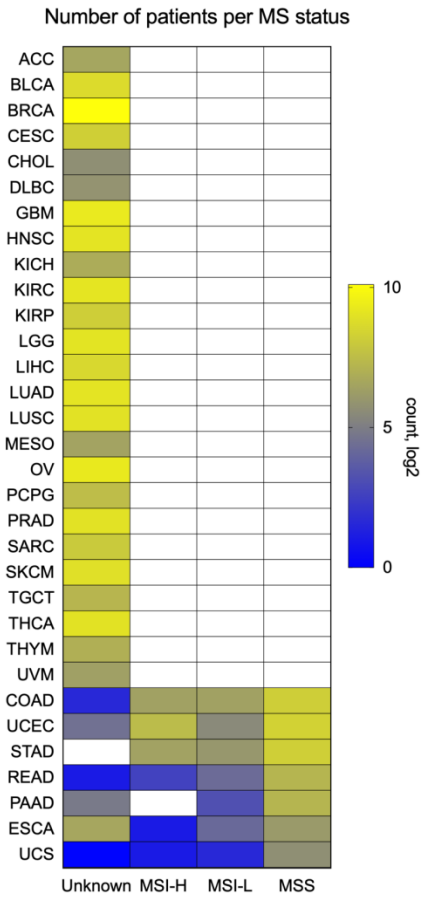

B.

	Unknown	MSI-H	MSI-L	MSS
COAD	0.00 (3)	0.18 (83)	0.18 (83)	0.63 (292)
UCEC	0.02 (22)	0.30 (170)	0.08 (44)	0.58 (324)
STAD	0.00 (0)	0.19 (85)	0.14 (63)	0.67 (295)

C.

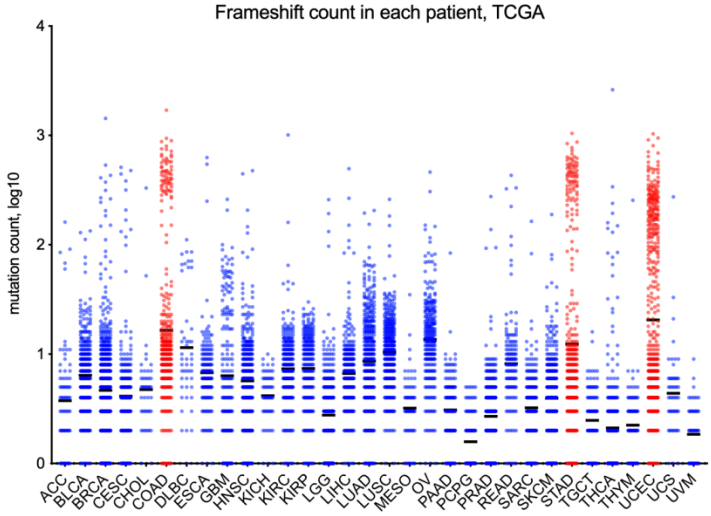

D.

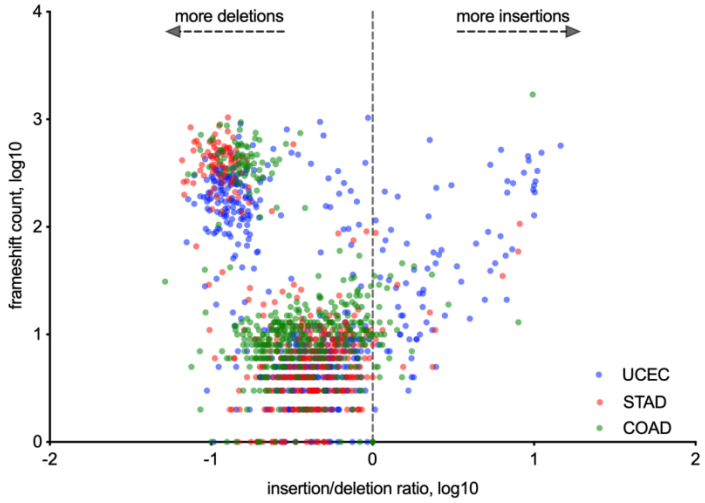

E.

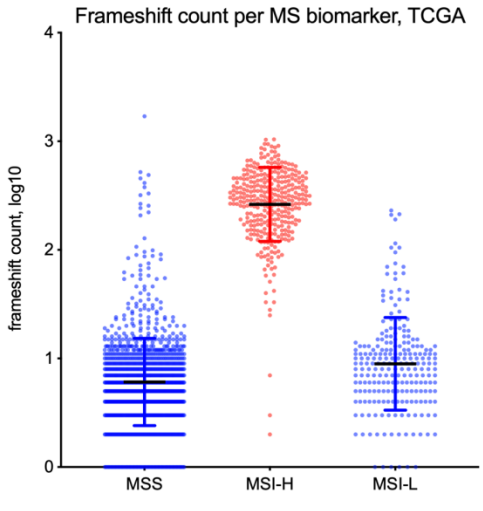

618

619 **Figure 1**. Microsatellite instability is detected in COAD, STAD and UCEC tumors in TCGA.
620 Majority of MSI-H frameshifts are deletions. **A.** Quantification of patients with microsatellite
621 instable (MSI) tumors according to biomarker, applied by TCGA. MSI-H - MSI-high, MSI-L - MSI-
622 low, MSS - MS-stable, and Unknown – undetermined MS status. **B.** Table, showing the fraction
623 (absolute number) of patients with UCEC, COAD and STAD tumors identified as MSI-H, MSI-L,
624 MSS or Unknown. **C**. Frameshift (fs-) load (Y-axis, log10) in different tumor types across TCGA.
625 **D.** Comparison of fs-load (Y-axis, log10) with insertion-deletion ratio (X-axis, log10) in COAD,
626 STAD and UCEC tumors. **E**. Segregation of fs-load by MS biomarker.
627

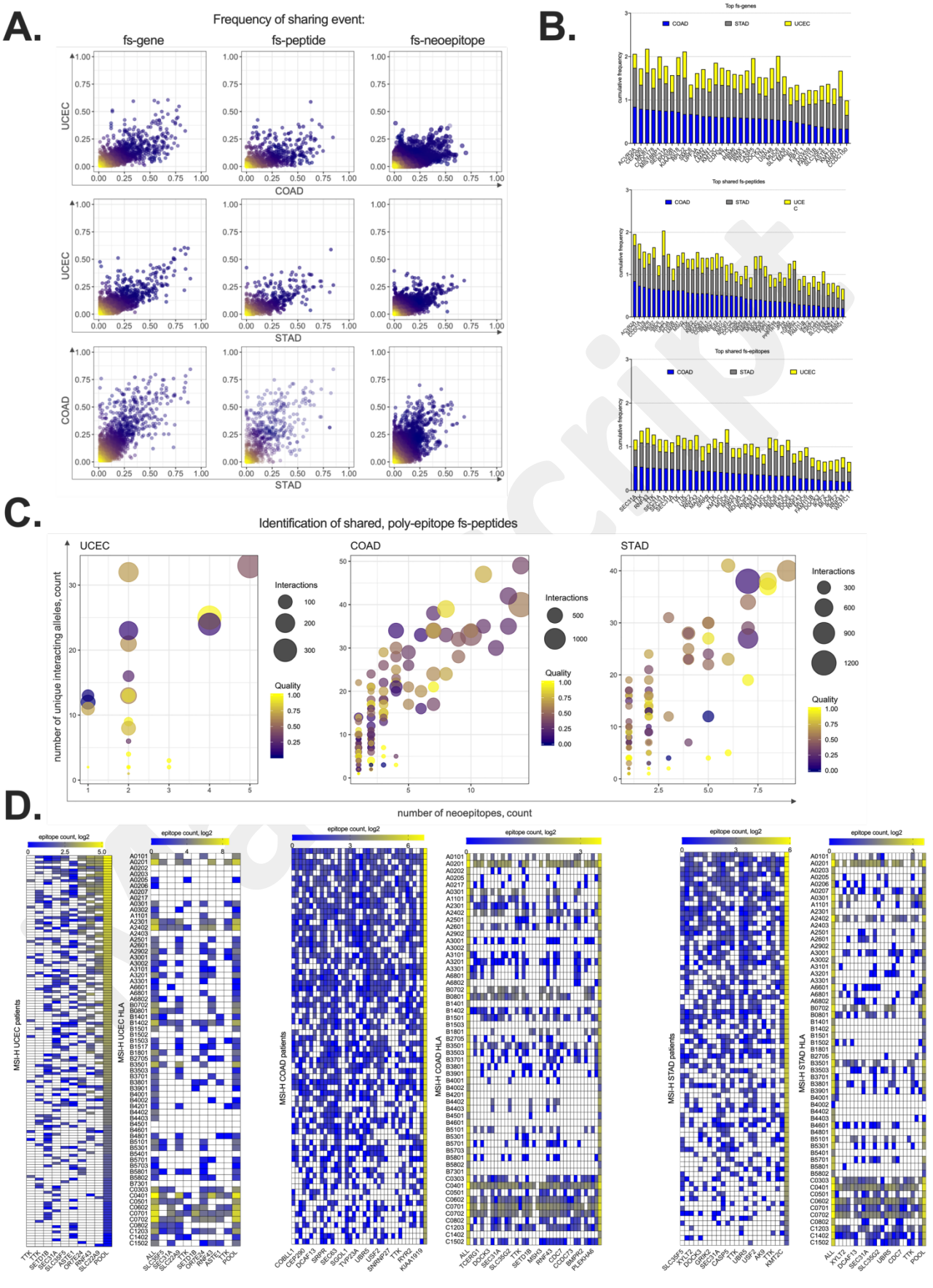

628

Figure 2. Frequencies of shared, fs-events in STAD, COAD and UCEC MSI-H tumors. Greedy pipeline for identification of shared, fs-peptides in MSI-H tumors. **A.** Scatterplots of patient frequencies of frameshifted genes (LEFT), fs-peptides (CENTER) and fs-epitopes (RIGHT) in UCEC, STAD and COAD MSI-H tumors. **B.** Cumulative frequency histograms, showing most frequently mutated genes via indels (TOP); genes, mutated by shared fs-peptide (CENTER); genes, encoding shared fs-neoantigens (BOTTOM). **C.** Three scatterplots showing selection procedure for identification of shared fs-peptides in UCEC (LEFT), COAD (CENTER) and STAD (RIGHT) patients. Each dot represents fs-peptide with the frequency of sharing above 20% in the patient cohort. Amount of predicted 9-mer epitopes per peptide (X-axis) is plotted against a number of predicted interacting HLA alleles (Y-axis). Size of the circle represents total number of predicted interactions between HLA-alleles and encoded epitopes. Color of the dot reflects the ratio of "PASS"ed fs-mutations to total number of called fs-mutations, according to somatic callers used by TCGA consortium. **D.** Quantification of T cell epitopes (log2 scale) derived from shared fs-peptides (columns) per each patient (rows, odd heatmaps) or each HLA allele (rows, even heatmaps) found in UCEC, COAD and STAD MSI-H cohorts.

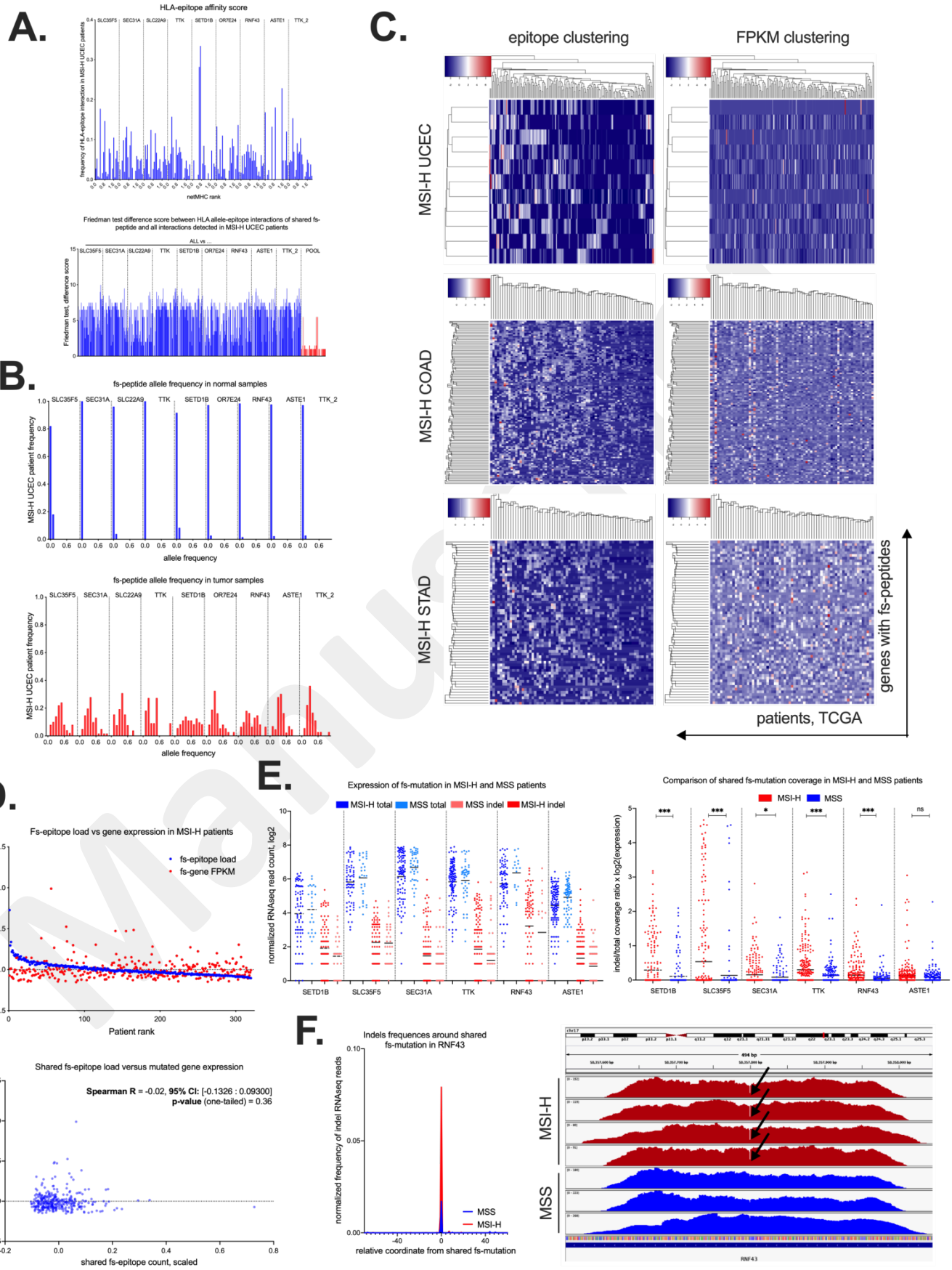

645

Figure 3. Genomic and expression properties of shared, immunogenic fs-mutations in MSI-H UCEC tumor. Neoantigen quality of predicted epitopes. **A.** TOP – Distribution of predicted HLA allele-epitope interaction ranking scores (NetMHC v3.4/v4.0), derived from nine shared fs-peptides in MSI-H UCEC. BOTTOM – Friedman difference score, measuring the difference between total amount of HLA-allele epitope interactions found in MSI-H UCEC patients (ALL) and either sum of epitope-allele interactions per each fs-peptide separately, or pooled together (POOL). Each bar represents the difference score between number of predicted epitopes per each HLA allele. **B.** tumor allele frequency of nine shared frameshift mutations in normal (TOP) and tumor (BOTTOM) tissues of MSI-H UCEC TCGA patients. **C.** Unsupervised hierarchical clustering of shared fs-mutations (LEFT) and corresponding FPKM values of frameshifted genes (RIGHT) in MSI-H UCEC (TOP), COAD (CENTER) and STAD (BOTTOM) tumors. Patients plotted in columns, genes plotted in rows. **D.** TOP – scatterplot of shared fs-load and corresponding gene expression per each MSI-H patient. BOTTOM – correlation plot between scaled fs-load and expression. **E**. Normalized expression of nine shared fs-mutations in MSI-H UCEC patients. LEFT – normalized expression of total and indel-containing reads spanning the genomic loci of six shared fs-mutations. RIGHT – ratio of indel to total read count spanning the microsatellite region in MSI-H and MSS patient cohort of UCEC, STAD and COAD tumors. Statistical significance is derived from non-parametric Mann-Whitney two-tailed test. **F.** Representative example of shared frameshift detected in RNAseq datasets. LEFT – normalized frequency of fs-mutation in RNF43 within 100 nucleotide genomic loci: 50 nt upstream and 50 nt downstream the shared frameshift in MSI-H and MSS RNAseq samples. RIGHT – RNAseq read histograms around the shared frameshift in RNF43 from MSI-H (red) and MSS (blue) patients. The 1-nucleotide long drop in RNAseq read coverage at the site of shared frameshift is indicated with an arrow.

669

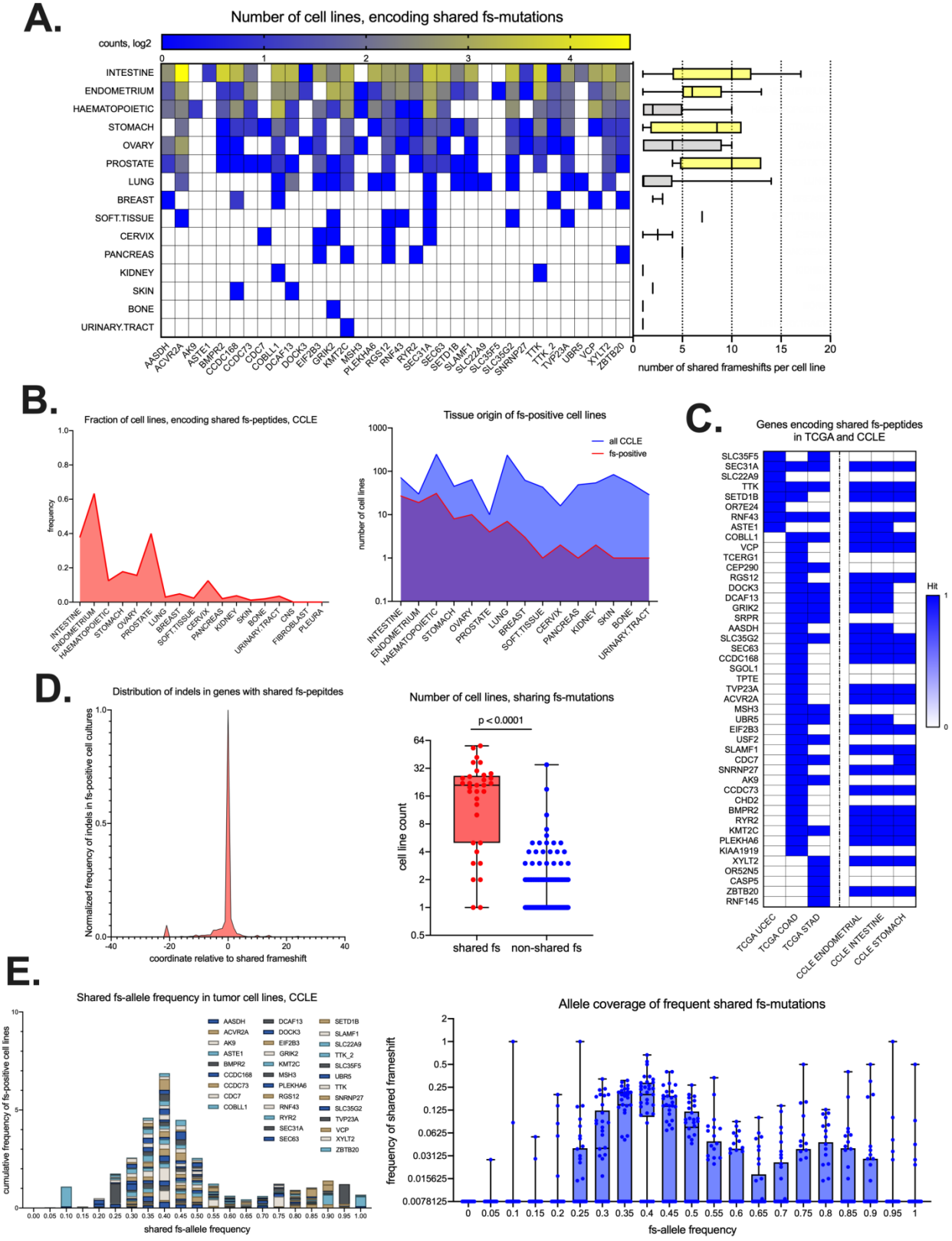

670

671 **Figure 4.** Detection of shared fs-mutations in cancer cell line encyclopedia (CCLE). **A.**
672 Quantification of shared fs-mutations in cell lines per tissue of tumor origin and per each
673 frameshifted gene. Histogram plot on the left shows number of shared fs-mutations per cell line.
674 **B.** General statistics of cell lines, encoding shared fs-peptides. LEFT – fraction of cell lines,
675 positive for shared fs-mutation, per each tissue type. RIGHT – Absolute number of cell lines
676 with detected shared fs-mutation compared to total number of cell lines in CCLE. Cell lines are
677 sorted according to tissue origin. **C.** Gene and tumor specificity of shared fs-mutations in TCGA
678 and CCLE. **D.** Distribution of all detected indels in genes with shared fs-mutations (34 genes in
679 CCLE). LEFT – metagene, showing normalized frequency of all detected indels in 34 genes,
680 around shared fs-mutation. RIGHT – t-test of number of cell lines encoding shared fs-mutation
681 versus all other fs-mutations, detected in selected 34 genes. **E.** fs-allele frequency in WES
682 samples of shared fs-mutation positive cell lines. LEFT – cumulative histogram plot, showing fs-
683 allele frequency of each shared fs-mutation per gene of origin. RIGHT – box-plot of fs-allele
684 frequency plotted against frequency of fs-mutation in the pool of fs-positive cell lines.
685

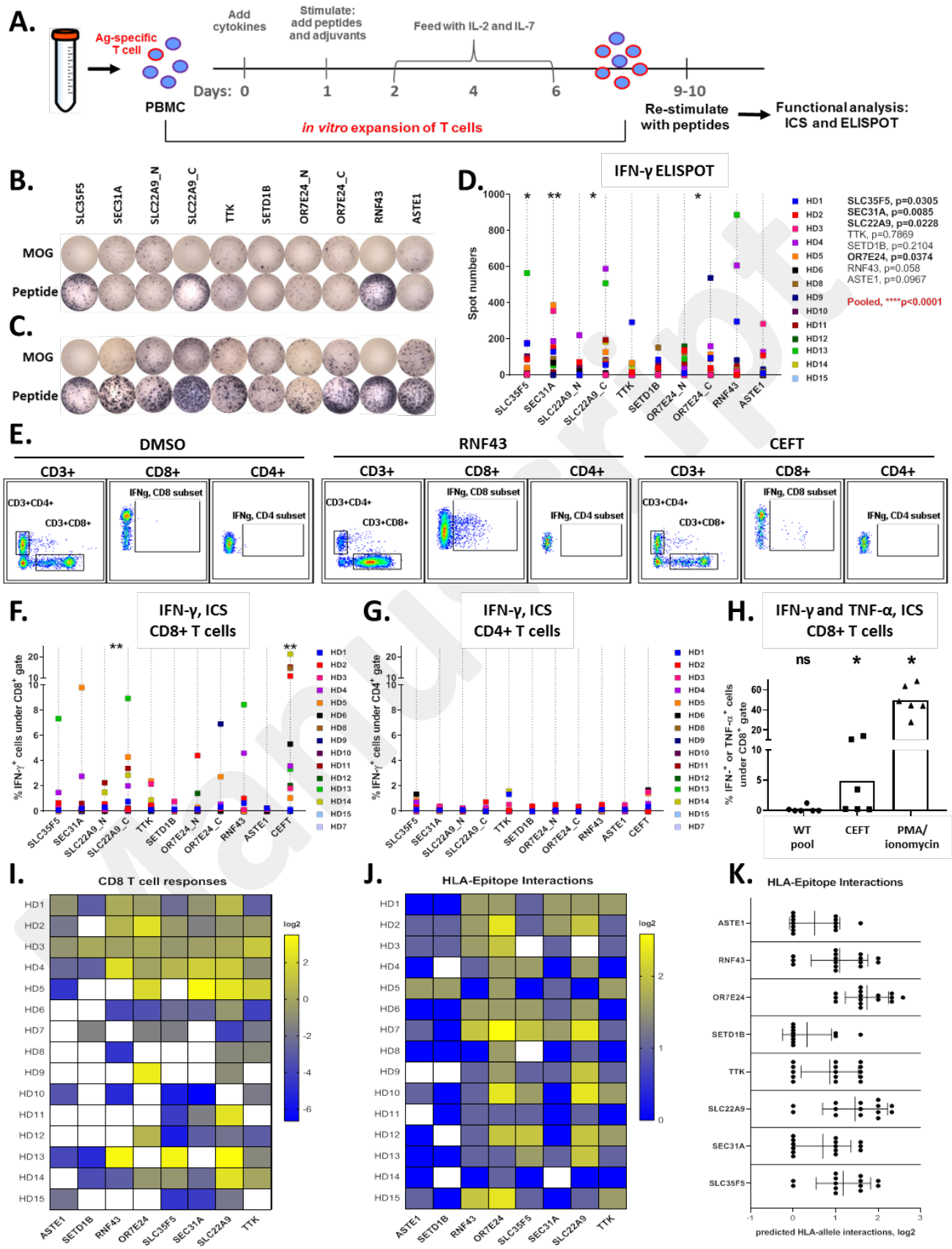

686

687 **Figure 5.** Shared fs-peptides predicted from UCEC MSI-H patients elicit T cell responses. **A.** An
688 overview of T cell immunogenicity assay used to evaluate antigen-specific T cell responses.
689 PBMCs from healthy donors (HD) were expanded *in vitro* following stimulation with fs-peptide
690 OLPs as shown in supplementary figure 7. Expanded T cells ($5x10^4$ cells/well) were re-
691 stimulated with either the peptide pool they were expanded with or the control peptide pool
692 MOG. Representative IFN-γ ELISPOT images for **B.** HD13 or **C.** for selected responsive HD. **D.**
693 Summary of ELISPOT data (n=14). Statistical significance for MOG vs OLPs was evaluated by
694 Wilcoxon signed-rank test. **E.** Representative flow cytometry plots and summary of data (n=15)
695 for IFN-γ in **F.** CD8 and **G.** CD4 T cell subsets. Stimulation with CEFT was used as a control.
696 Statistical significance for DMSO vs OLPs was evaluated by Wilcoxon signed-rank test.
697 **p=0.0032 for SLC22A9 and **0.0031 for CEFT. **H.** Frequency of IFN-γ or TNF-α producing
698 CD8+ T cells upon stimulation with WT OLP pool. CEFT and PMA/Ionomycin stimulation was
699 used as a control. The spot numbers and % IFN-γ values were calculated by subtracting the
700 values obtained after MOG or DMSO stimulation from the values after OLP pool stimulation
701 and negative values were set to zero. **I.** Summary of log2 transformed data for IFN-γ /TNF-α
702 response by CD8+ T cells against fs-peptides. **J.** and **K.** Quantification (log2 transformed) of HLA
703 allele-epitope interactions for each subject per fs-peptide. Interactions were counted when IC50<500
704 or percentile rank<2.
705

706 # Supplementary Information

A.

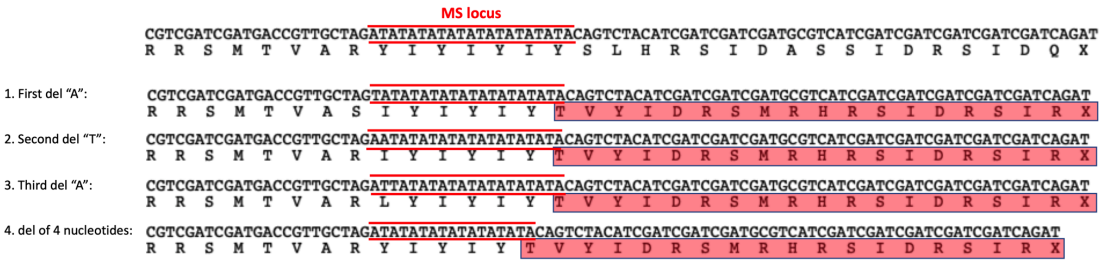

B.

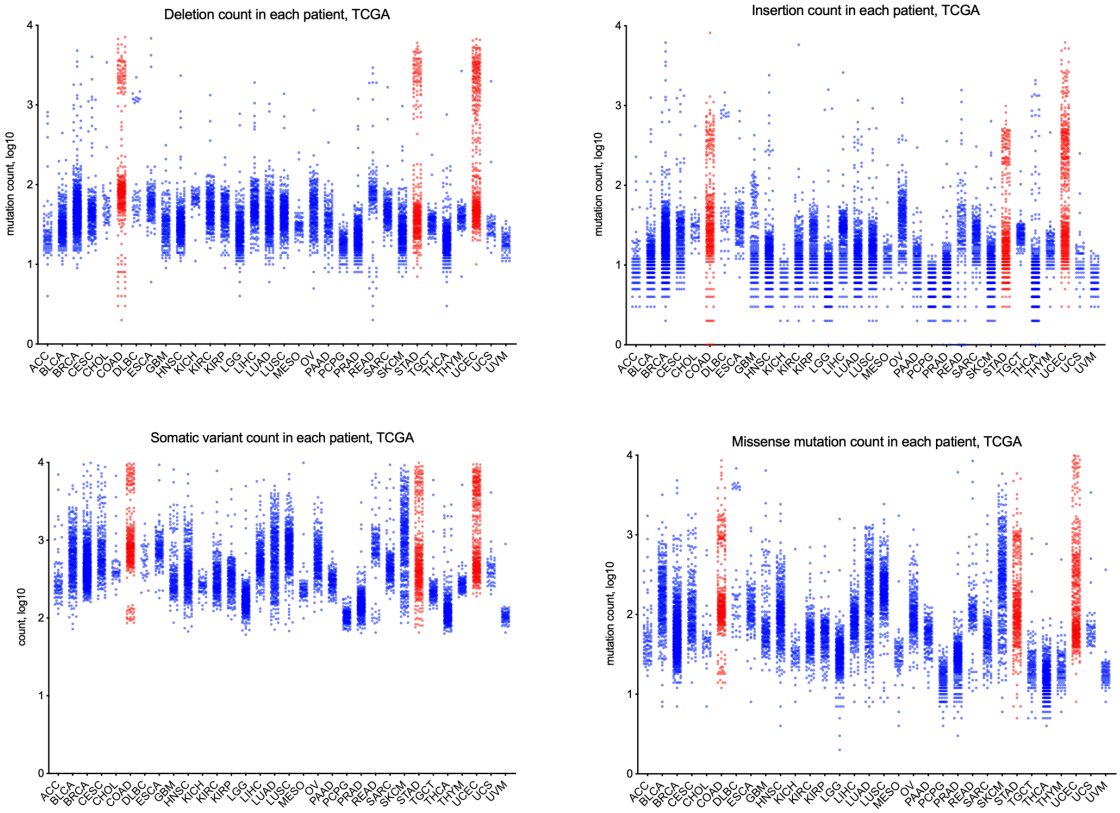

C.

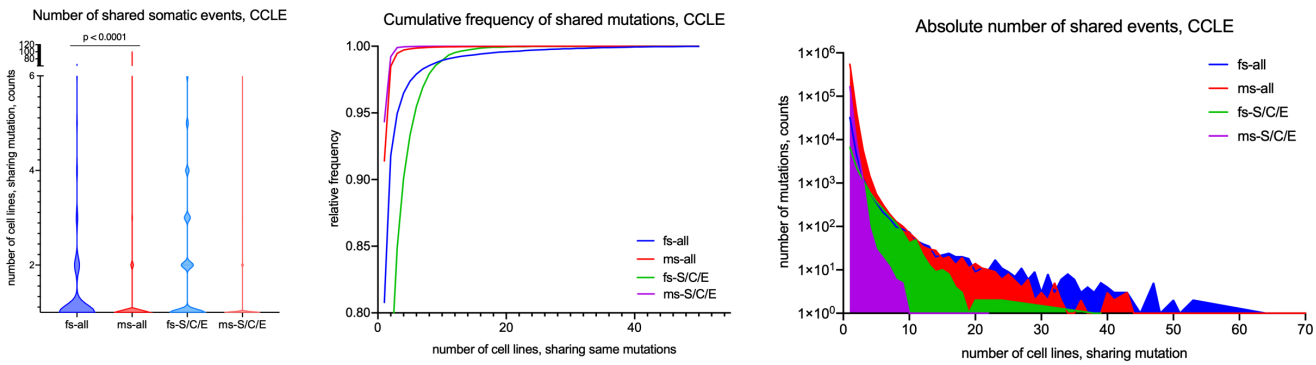

707

708 **Supplementary Figure 1**. Mutational analysis of TCGA. **A.** Hypothetical example of multiple
709 deletions happening in microsatellite region and leading to identical frameshift (fs-)peptide. **B.**
710 Comparison of frequencies of shared somatic indels and missense point mutations in human cancer
711 cell lines from CCLE. LEFT – number of cancer cell lines, sharing same fs-mutation or same
712 missense point mutation from all CCLE (fs-all and ms-all respectively) or from stomach, colon and
713 endometrium cell lines (fs-S/C/E and ms-S/C/E respectively). Statistical significance derived from
714 non-parametric Mann-Whitney, one-tailed test. CENTER – cumulative frequency plot of shared
715 indel and missense mutation from all CCLE (fs-all and ms-all respectively) or from stomach, colon
716 and endometrium cell lines (fs-S/C/E and ms-S/C/E respectively). RIGHT – absolute number of
717 shared mutations in cancer cell lines from all CCLE (fs-all and ms-all respectively) or from stomach,
718 colon and endometrium cell lines (fs-S/C/E and ms-S/C/E respectively). **C.** Mutational load across
719 different tumor types in TCGA. From left to right, top to bottom: deletion, insertion, somatic variant
720 and missense mutation load.
721

A.

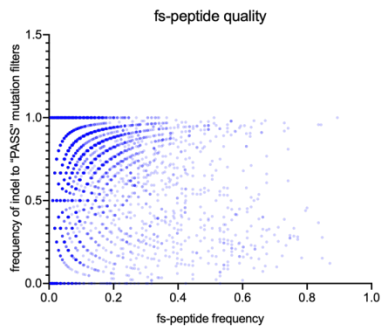

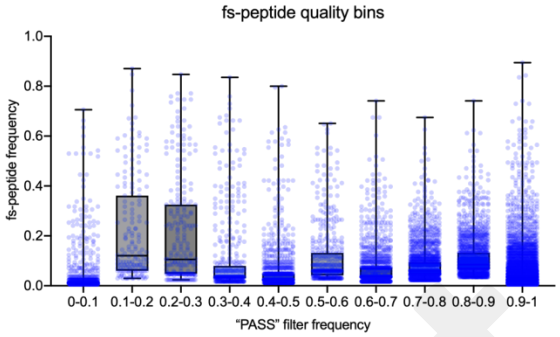

B.

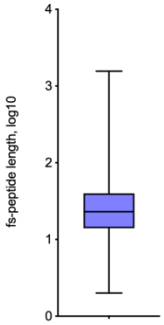

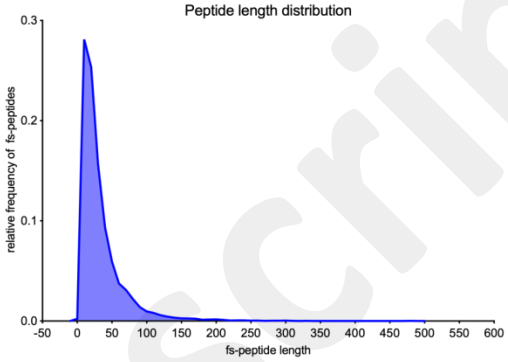

C.

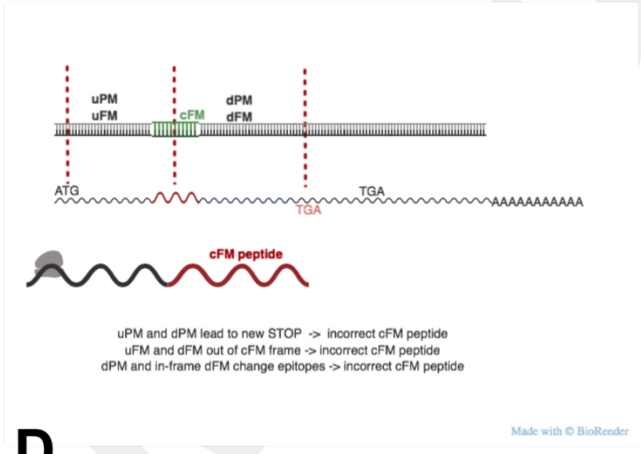

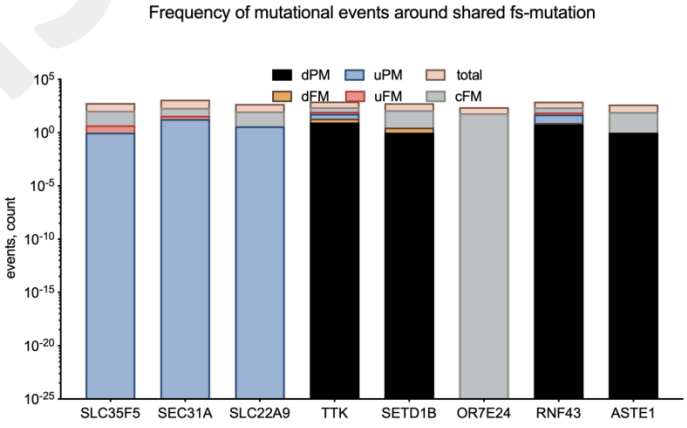

D.

$$P_{ccFM \mid cFM} = 1 - [\,(P_{uPM \mid cFM} + P_{dPM \mid cFM}) \times P_{A,T,G} \times P_{STOP \mid A,T,G} + (P_{dPM \mid cFM} \times P_{missense} + P_{dFM \mid cFM} \times P_{inframe}) \times P_{epitope} + (P_{uFM \mid cFM} + P_{dFM \mid cFM}) \times P_{outframe}\,] \times P_{linkage}$$

$$P_{ccFM \mid cFM} = 1 - [\,(P_{uPM \mid cFM} + P_{dPM \mid cFM}) \times 3/4 \times 3/27 + (P_{dPM \mid cFM} \times 2/3 + P_{dFM \mid cFM} \times 1/3) \times \Sigma_{k=1}^{n} C^{n}_{k} \times (7/len_{FM})^{k} + (P_{uFM \mid cFM} + P_{dFM \mid cFM}) \times 2/3\,] \times 1/2$$

GENE	PccFM | cFM
SLC35F5	0.98
SEC31A	0.92
SLC22A9	0.99
TTK	0.79
SETD1B	0.99
OR7E24	1.00
RNF43	0.82
ASTE1	1.00

722

Supplementary Figure 2. Properties of predicted frameshift peptides. **A.** Distribution of quality metrics for each frameshift mutation detected in MSI-H patients. LEFT – ratio of "PASS" mutation calls for each frameshift, plotted against fs-mutation frequency. RIGHT – box-plot of frameshift frequency in MSI-H patient cohort per 10%-quality bin. The least shared fs-events are the most confident, while majority of shared fs-mutations are within 10-50% "PASS" quality range. **B.** Box plot (LEFT) and distribution (RIGHT) of fs-peptide frequency as function of its length. Most frequent fs-peptides are in 15-50 aminoacid residue range. **C, D.** Estimation of correctness of nine shared frameshift peptides in MSI-H UCEC population. In the reduced approximation, any upstream mutation (upstream fs-mutation uFM or upstream point mutation uPM) may alter the fs-peptide if uFM appears somewhere between start codon and predicted shared fs-mutation or if uPM leads to an abortive stop codon; alternatively, any downstream mutation (downstream fs-mutation dFM or downstream point mutation dPM) may alter shared fs-peptide if dFM happens between shared mutation and novel stop codon, defined by the frame of fs-peptide or if dPM happens within predicted T cell epitope or leads to abortive stop codon. **C.** LEFT: representation of upstream and downstream mutagenesis, which can be detrimental to the predicted fs-peptide; RIGHT – quantification of detrimental events around shared fs-peptides. **D.** LEFT: probabilistic function to estimate conditional probability of fs-peptide being correct given that this fs-mutation is happened; RIGHT: estimated posterior probabilities for each nine shared fs-peptides.

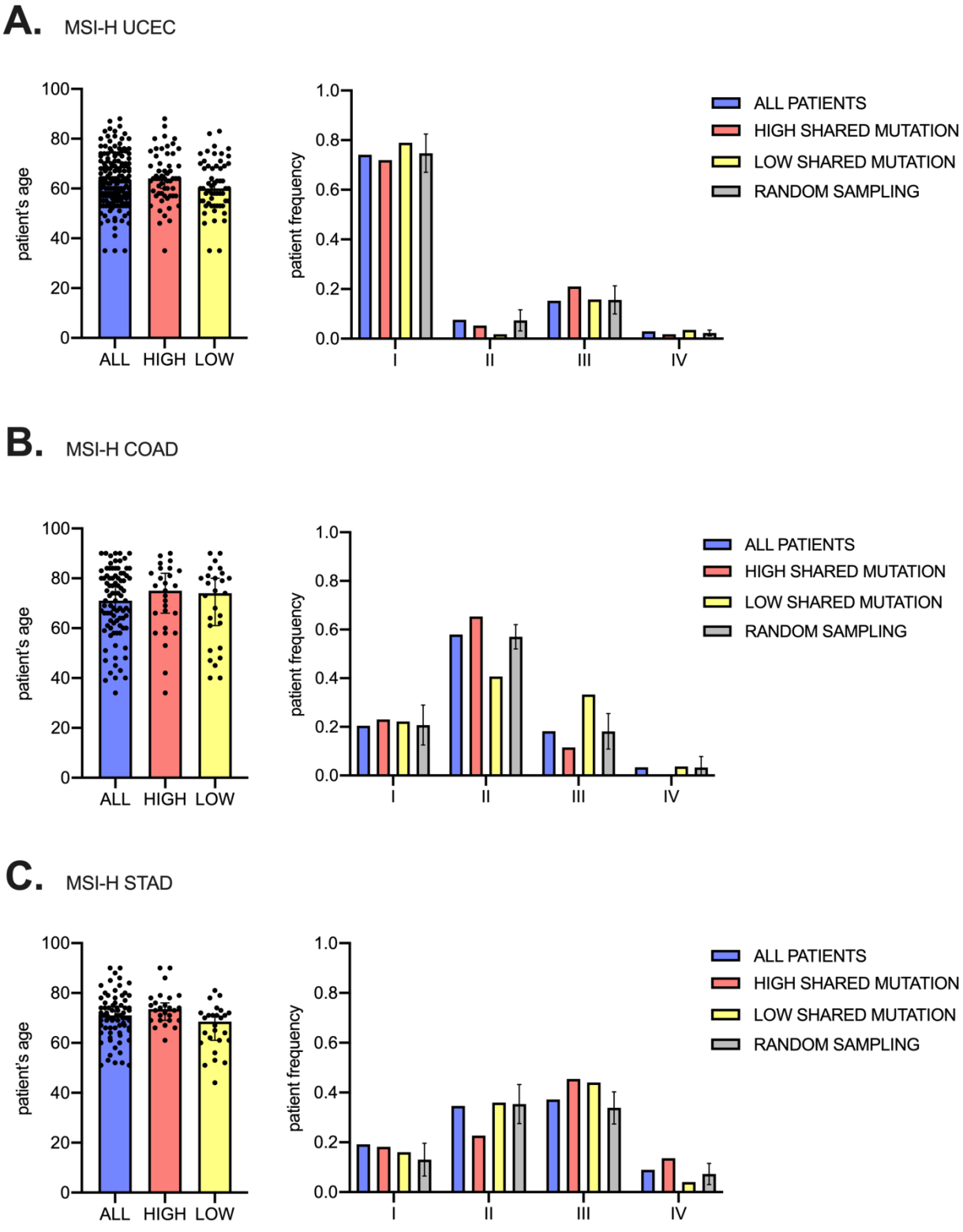

742

743 **Supplementary Figure 3.** Distribution of patient's age and tumor stages based on shared fs-epitope
744 load in MSI-H tumors, TCGA. **A.** LEFT – distribution of patient's age in all, shared fs-epitope high
745 and shared fs-epitope low patients' cohort, MSI-H UCEC tumor type. RIGHT – patients' frequency
746 across tumor stages in the same cohorts, as above. **B.** LEFT – distribution of patient's age in all,
747 shared fs-epitope high and shared fs-epitope low patients' cohort, MSI-H COAD tumor type. RIGHT
748 – patients' frequency across tumor stages in the same cohorts, as above. **C.** LEFT – distribution of
749 patient's age in all, shared fs-epitope high and shared fs-epitope low patients' cohort, MSI-H STAD
750 tumor type. RIGHT – patients' frequency across tumor stages in the same cohorts, as above.
751

A. MSI-H UCEC

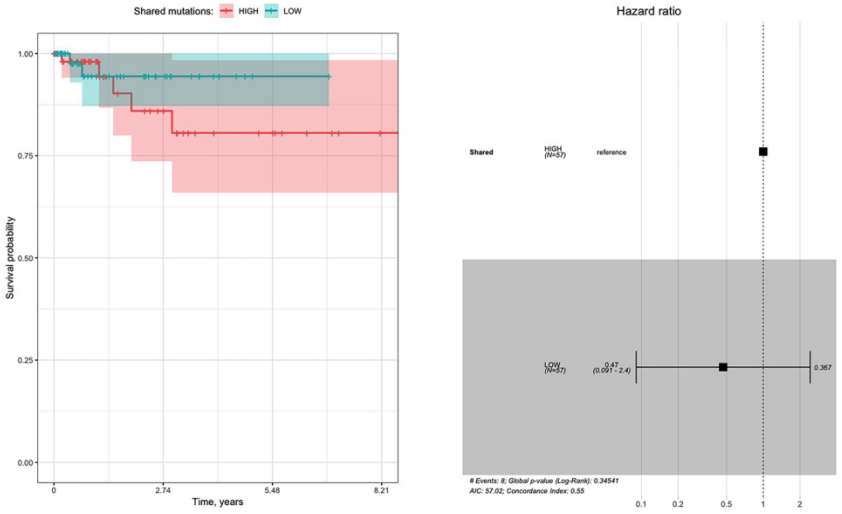

Log-Rank p-value: 0.34541

Hazard ratio: 0.47
(95% CI: 0.091 - 2.4)

B. MSI-H COAD

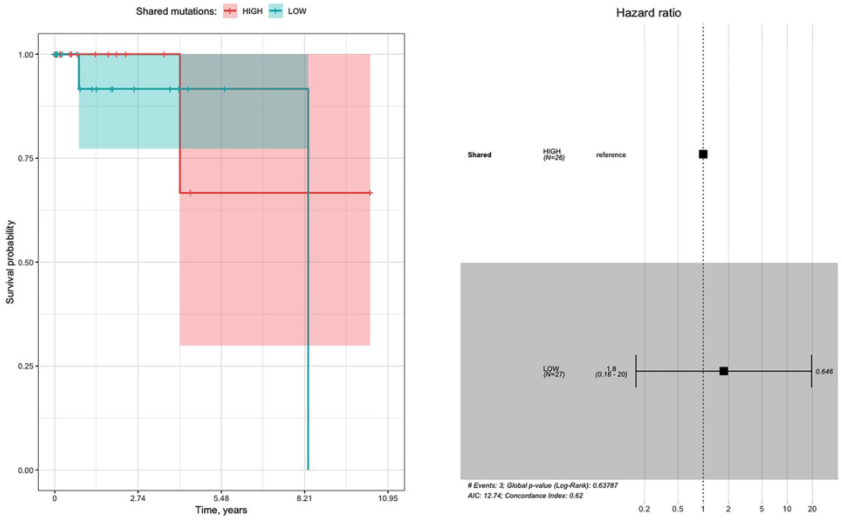

Log-Rank p-value: 0.63787

Hazard ratio: 1.8
(95% CI: 0.16 - 20)

C. MSI-H STAD

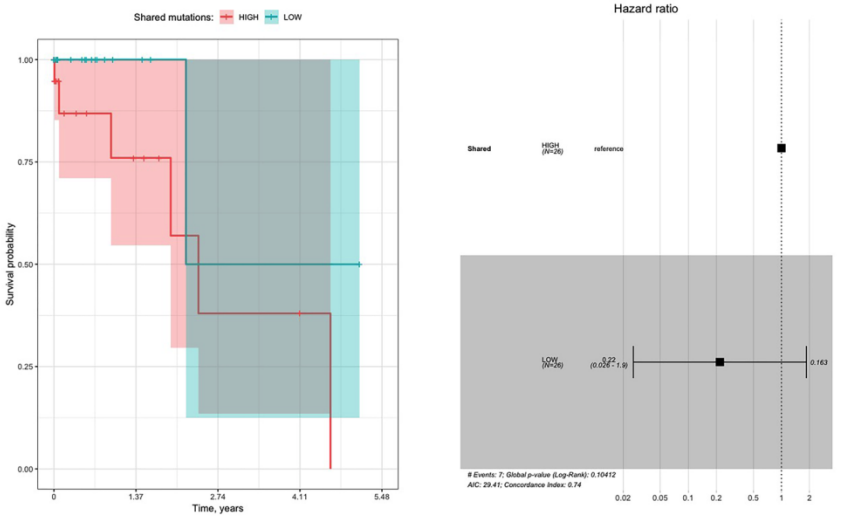

Log-Rank p-value: 0.10412

Hazard ratio: 0.22
(95% CI: 0.026 - 1.9)

752

753 **Supplementary Figure 4.** Kaplan-Meier plot of survival analysis (LEFT) and Cox's proportional
754 hazards model (RIGHT) of MSI-H UCEC (**A**), COAD (**B**) and STAD (**C**) patients, segregated by
755 shared fs-epitope load (HIGH vs LOW).
756

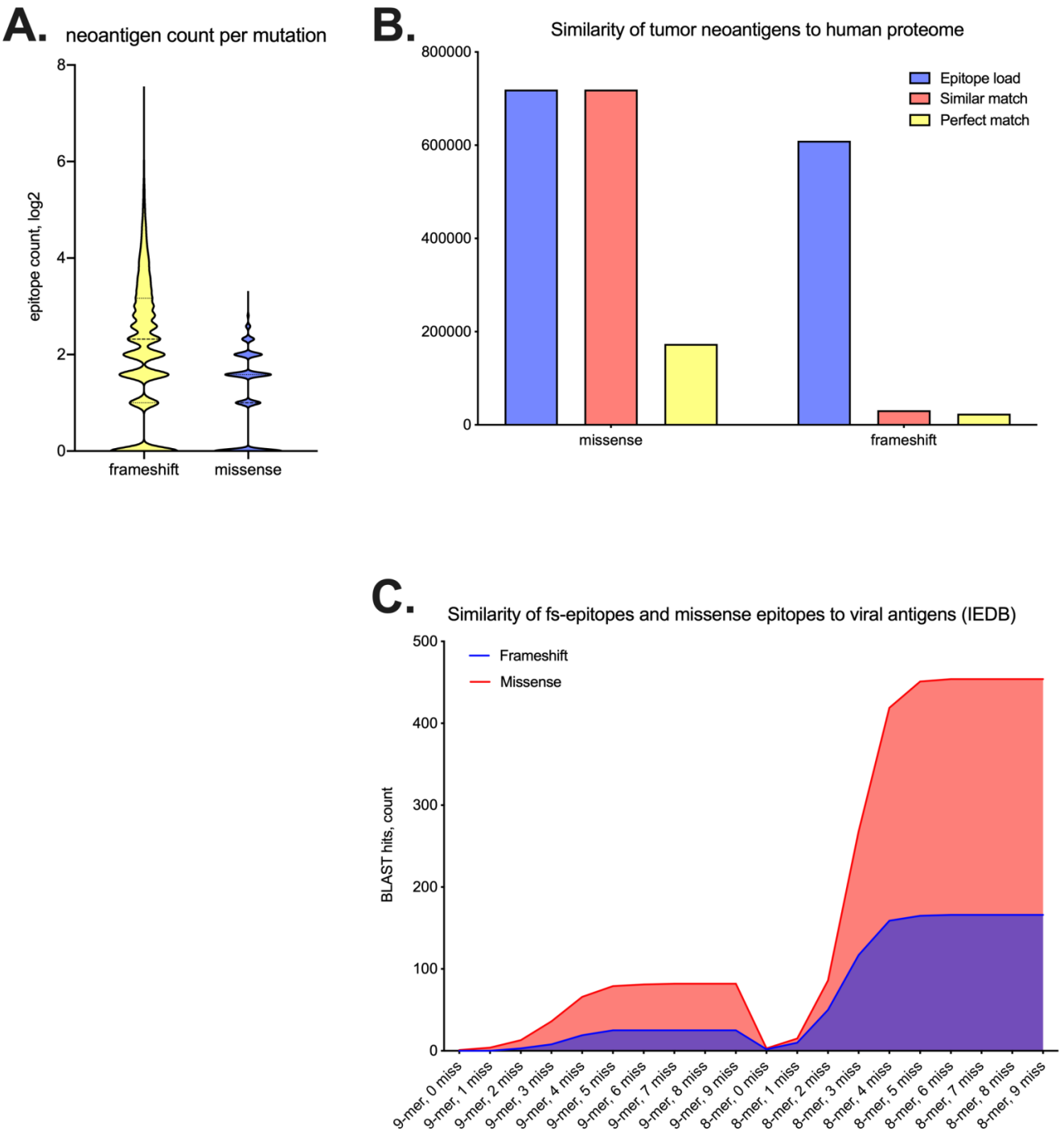

Supplementary Figure 5. Comparison of missense epitopes and fs-epitopes in MSI-H patients with human proteome and annotated viral epitopes (IEDB). **A.** Quantification of epitopes per missense or frameshift mutation. On average, frameshift mutation generates 4 epitopes, while missense - 2. **B.**

761 Mapping missense and fs-epitopes back to human proteome (ensemble, 2016). "Epitope load"
762 indicates total amount of predicted neoantigens from missense and frameshift mutations; "Similar
763 match" shows number of epitopes, successfully aligned to human proteome by sequence of 8 non-
764 gapped aminoacid residues, allowing 1 mismatch; "Perfect match" shows number of epitopes,
765 perfectly matched to human proteome by sequence of 9 non-gapped aa with no mismatches. **C.**
766 BLAST comparison of missense epitopes and fs-epitopes with viral epitopes from IEDB, allowing
767 different number of mismatches. Missense-derived epitopes are more similar to viral epitopes then
768 frameshift-derived on average.
769

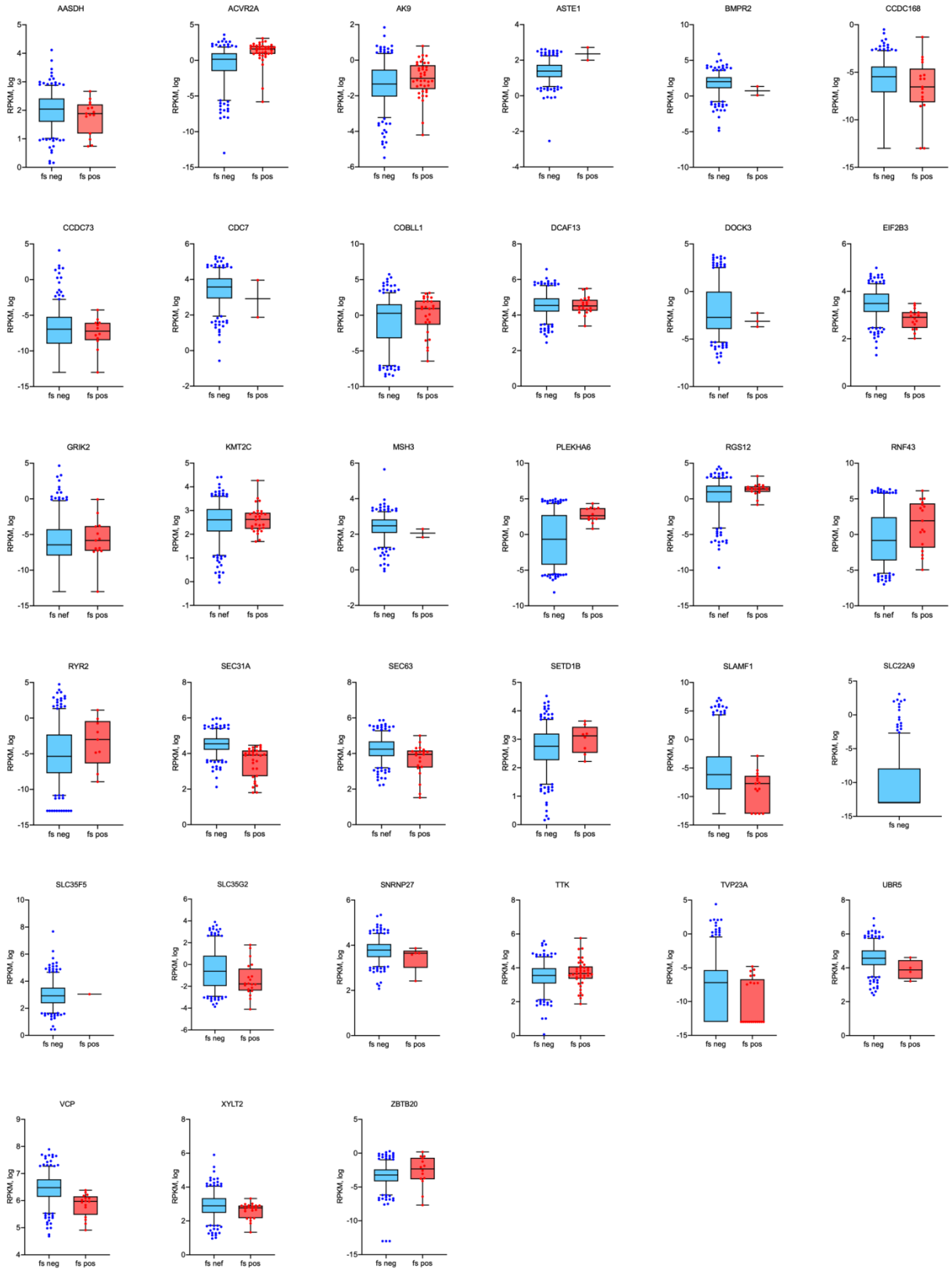

770

771 **Supplementary Figure 6.** RNA expression (RPKM, log2) of genes, carrying shared fs-mutation in

772 cell lines derived from CCLE. Each box-plot represents RPKM expression of gene of interest in

773 shared fs-negative and shared fs-positive cell lines.

774

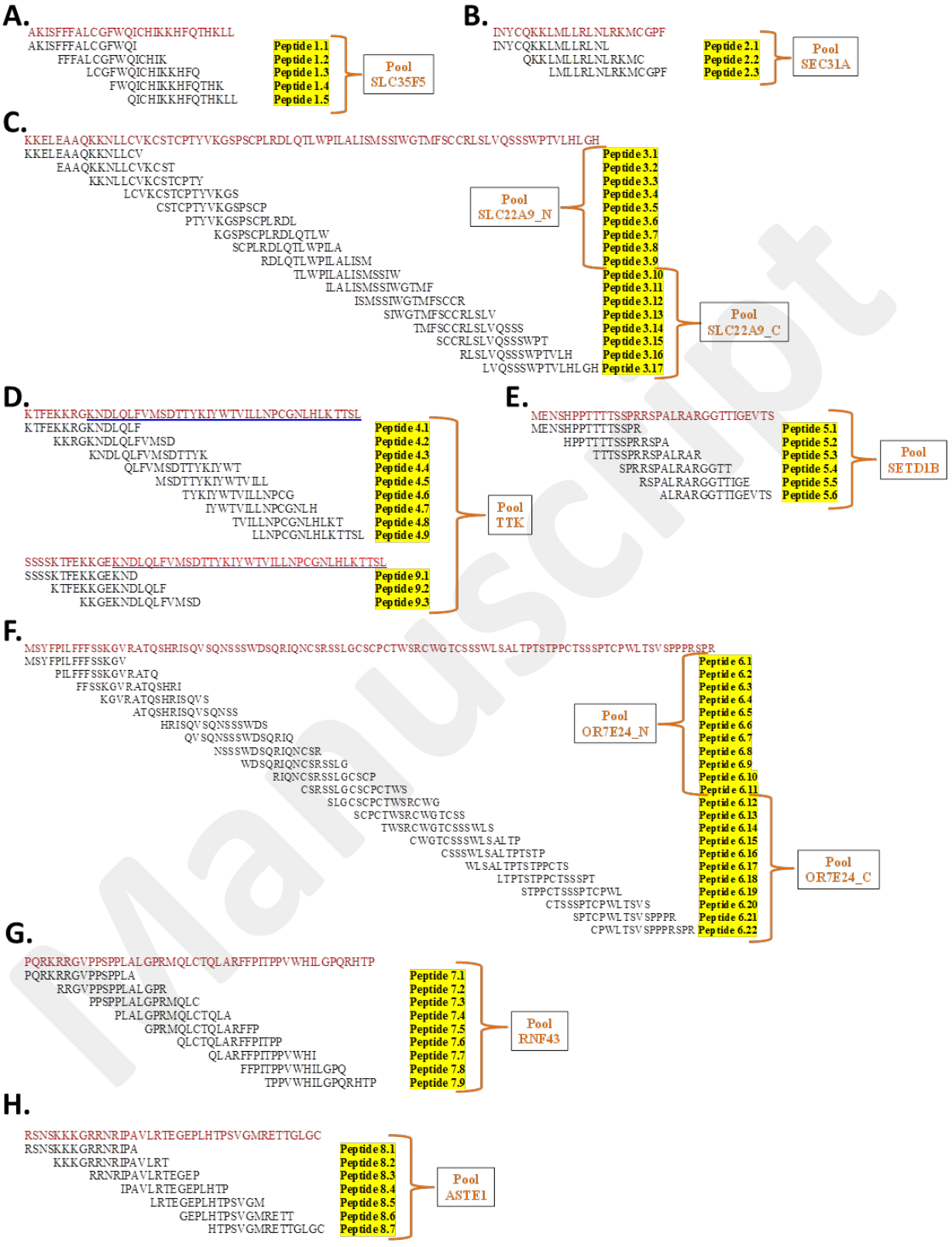

776 **Supplementary Figure 7**. Peptide design. 15-mer overlapping peptides spanning the upstream
777 8aa WT sequence and the entire mutated fs-peptide were synthesized for the predicted nine
778 shared fs-peptides from MSI-H UCEC. Peptide pools as they were utilized in the
779 immunogenicity assays were denoted. **A.** SLC35F5, **B.** SEC31A, **C.** SLC22A9**, D.** TTK**, E.**
780 SETD1B, **F.** OR7E24, **G.** RNF43, **H.** ASTE1.
781

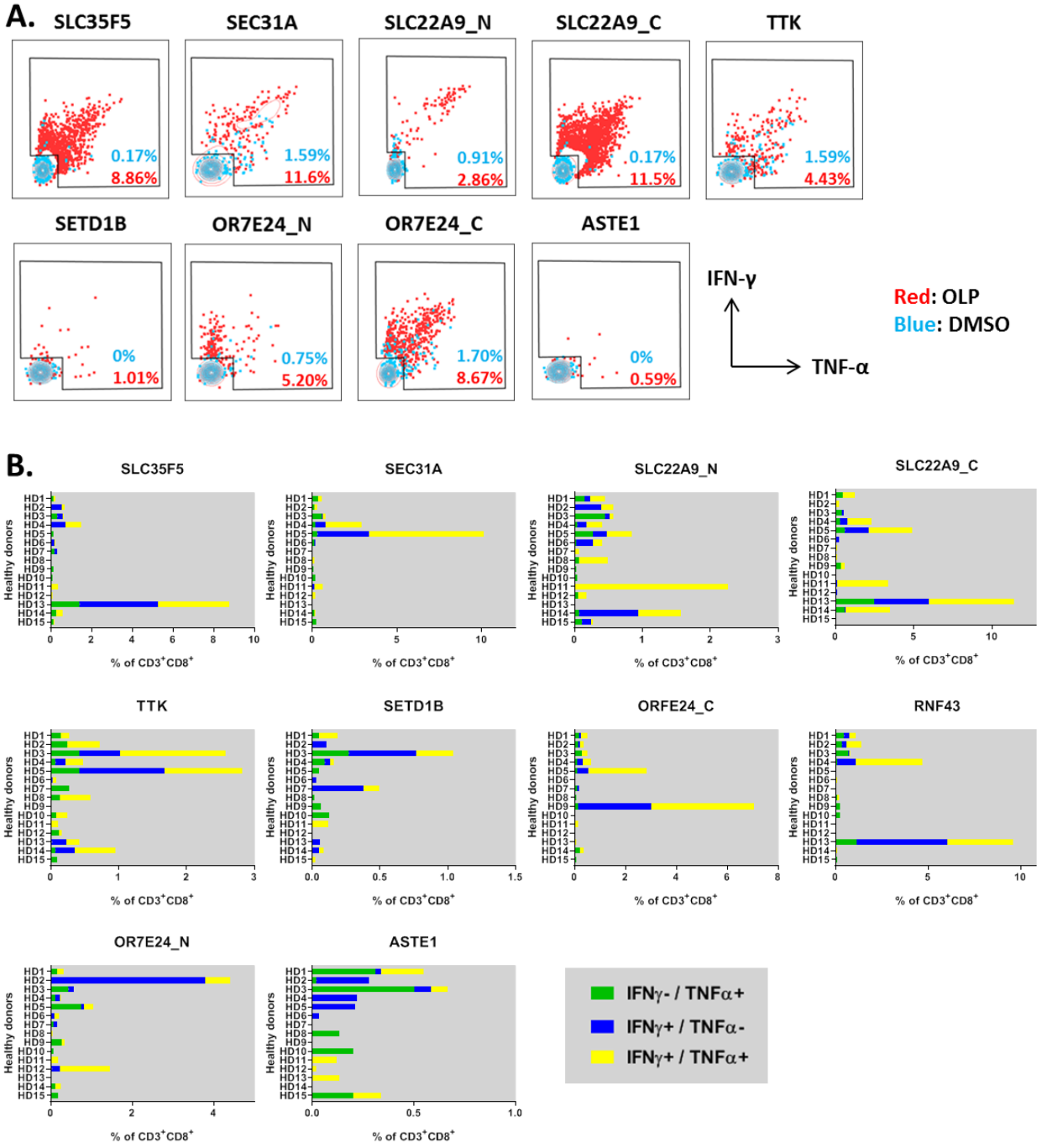

782

783 **Supplementary Figure 8.** Fs-peptide-specific T cells are polyfunctional. PBMCs from healthy

784 donors (HD) were expanded *in vitro* following stimulation with fs-peptide OLPs. DMSO was

785 used vehicle control. **A.** Representative flow cytometry overlay plots for IFN-γ (y axis) and

786 TNF-α (x axis) production by CD8+ T cells. Cytokine production upon OLP or DMSO

787 stimulation was shown in red or blue, respectively. **B.** Frequencies of CD8+ T cells producing
788 IFN-γ or TNF-α in response to each fs-peptide OLP pool were plotted for each subject. Green
789 denotes HD producing only TNF-α, blue denotes HD producing only IFN-γ and yellow denotes
790 HD producing both IFN-γ and TNF-α. % IFN-γ values were calculated by subtracting the values
791 obtained after DMSO stimulation from the values after OLP pool stimulation and negative
792 values were set to zero.